Trouble with the minimal renormalizable SO(10) GUT

Kateřina Jarkovská,[*] Michal Malinský,[†] and Vasja Susič[‡]

*Institute of Particle and Nuclear Physics, Faculty of Mathematics and Physics, Charles University in Prague,
V Holešovičkách 2, 180 00 Praha 8, Czech Republic*

We scrutinize the physical viability of the minimal nonsupersymmetric SO(10) grand unified theory with the scalar sector $\mathbf{45} \oplus \mathbf{126} \oplus \mathbf{10}_{\mathbb{C}}$, in which the unified symmetry is broken by the former two representations, and a realistic Yukawa sector is supported by the last two. Alongside the known issue of a relatively low grand unified theory scale (and thus overly fast proton decay) encountered in minimally fine-tuned scenarios, we identify a very general problem of the model: the inability to properly accommodate a Standard-Model-like low-energy Higgs doublet in the perturbative regime.

I. INTRODUCTION

The renormalizable SO(10) grand unified theory (GUT) in which the unified gauge symmetry breaking is triggered by the 45-dimensional adjoint scalar, followed by the rank reduction imposed by a 126-dimensional five-index antisymmetric scalar representation, has recently received quite some attention [1–13] as a candidate for a minimal potentially realistic and calculable grand unified model of possible baryon-number violating (BNV) phenomena like proton decay.

What is meant by calculability here is namely the capacity of the model to admit relatively good estimates of the relevant proton decay widths that could be (at least in principle) comparable with the data from the new experimental facilities with detection masses in the hundreds of kiloton range (like Hyper-K [14,15] and DUNE [16,17]) that will get online by the end of this decade. The defining feature here is the robustness of the framework (and the theoretical calculations within) to different types of theoretical uncertainties emanating from several basic sources. These include the limited information about the relevant hadronic matrix elements, little grip on the flavor structure of the charged-current interactions involved, the proximity of the GUT and Planck scale, etc., see, e.g., [18,19].

While the first two of the listed issues can be at least partly avoided by improving the corresponding QCD

calculations (first) or focusing on flavor-blind observables (second), there is no simple way to avoid the emergence of uncertainties associated to Planck-scale-induced $d \geq 5$ operators. The most dangerous are those operators that smear the mass estimates of the GUT-scale vectors and scalars that mediate BNV processes. The prominent culprit among these is the $d = 5$ structure $F_{\mu\nu}F^{\mu\nu}\Phi/\Lambda$ (with Φ denoting a GUT-breaking scalar), which inflicts out-of-control shifts in the GUT-scale matching conditions and hence in estimates of mediator masses [20–22]. Remarkably, the minimal renormalizable SO(10) GUT advocated above is free from these concerns at leading order, owing to the general absence of the corresponding $d = 5$ cubic adjoint invariant. However, this beautiful feature is "compensated" by the need to consider the model at the fully quantum level, since it has no consistent classical counterpart [23–26].

In general, the relative rigidity of the $\mathbf{45} \oplus \mathbf{126}$ Higgs sector admits only two minimally fine-tuned [27,28] SO (10) symmetry breaking patterns potentially compatible with unification and proton-lifetime constraints [29]. They feature either a $SU(4)_C \times SU(2)_L \times U(1)_R$ or $SU(3)_c \times SU(2)_L \times SU(2)_R \times U(1)_{B-L}$ intermediate stage. However, a recent detailed analysis [13] revealed that only the former variant can be reasonably implemented as a consistent perturbative scenario, and even then only in a very narrow domain of the parameter space. Moreover, the corresponding prediction for the GUT scale falls well below 10^{15} GeV, and thus the concerns about proton lifetime are reiterated.

Nevertheless, even with such a strong observation at hand, there are still several routes to explore before proclaiming this scenario completely unphysical. (i) First, the unification constraints in [13] have been implemented at a one-loop level and a dedicated higher-loop analysis may in principle change them. It is known that this is unlikely

[*]jarkovska@ipnp.mff.cuni.cz
[†]malinsky@ipnp.mff.cuni.cz
[‡]susic@ipnp.mff.cuni.cz

055003-1

to happen in the class of minimally fine-tuned scenarios [29–31], but this option cannot be entirely ignored if the extended survival hypothesis [32] was not adhered to and some of the naturally heavy scalar multiplets were brought well into the desert [3,4]. (ii) Second, the results of the one-loop analysis of the $\mathbf{45} \oplus \mathbf{126}$ Higgs model in [13] cannot be passed on when it comes to physics, as there is a need for at least one more scalar representation [typically, a $\mathbf{10}$ of SO(10)] to accommodate a realistic Yukawa sector. Along with that, a new source of quantum effects that were not taken into account in [13] emerges from the $\mathbf{10}$.

Needless to say, due to the complexity of computing the one-loop spectrum even in the $\mathbf{45} \oplus \mathbf{126}$ simplified model [8,13], a general analysis of all the options under point (i) above (i.e., all possible combinations of accidentally light thresholds) would be extremely tedious and unlikely to bring any decisive result. However, as we argue in this paper, there seems to be a deeper and universal issue plaguing even the fully physical $\mathbf{45} \oplus \mathbf{126} \oplus \mathbf{10}_\mathbb{C}$ variant of the model when it comes to its low-energy effective structure, namely, there is a strong tension between the need to attain a light SM Higgs-like doublet and the perturbativity of the setting irrespective of what one does with the rest of the scalar sector.

The study is organized as follows: In Sec. II, we recapitulate the salient features of the minimal potentially realistic Higgs sector containing $\mathbf{45} \oplus \mathbf{126} \oplus \mathbf{10}_\mathbb{C}$, where the first two representations are involved in the symmetry breaking of GUT to SM symmetry, while the complex scalar $\mathbf{10}_\mathbb{C}$ together with the $\mathbf{126}$ admits a realistic Yukawa sector. The quantitative conditions for this to work are formulated in Sec. II B, and then scrutinized at tree level analytically in Sec. III and at one-loop level numerically in Sec. IV. We conclude in Sec. V. The technical details of the analysis are deferred to a set of Appendices.

II. THE $\mathbf{45} \oplus \mathbf{126} \oplus \mathbf{10}$ MODEL

In what follows we consider the SO(10) GUT model with the $\mathbf{45} \oplus \mathbf{126} \oplus \mathbf{10}_\mathbb{C}$ scalar sector, which is a minimal extension of the Higgs model from [13] by a complex $\mathbf{10}_\mathbb{C}$, thus potentially allowing for realistic Yukawa matrices. We stress that the extra $\mathbf{10}$ of SO(10) must be complex (equivalent to two copies of a real $\mathbf{10}$)—a point we discuss in more detail later in Sec. II B. In addition, the three generations of the Standard Model (SM) fermions (including a right-handed neutrino in each family) are embedded into three copies of the spinorial $\mathbf{16}_F$ in the usual way [33], while the gauge fields are present in the adjoint $\mathbf{45}_G$. The model under consideration is essentially the minimal renormalizable potentially realistic SO(10) GUT model.

For future reference, we list the scalar field content of this model in terms of SM irreducible representations in Table I. Each SM representation may be present with a multiplicity number greater than 1, and we specify the

TABLE I. The field content of the scalar sector $\mathbf{45} \oplus \mathbf{126} \oplus \mathbf{10}_\mathbb{C}$ of the SO(10) model under consideration in terms of the corresponding SM components. For each SM representation R its reality/complexity ($\mathbb{R}/\mathbb{C}$), multiplicity number and SO(10) origin are indicated. The "WGB" column specifies the number of massless copies corresponding to would-be Goldstone modes when SO(10) is completely broken down to $G_{321} \equiv \mathrm{SU}(3)_c \times \mathrm{SU}(2)_L \times \mathrm{U}(1)_Y$.

$R \sim G_{321}$	$\mathbb{R}/\mathbb{C}$	#	WGB	$\subseteq$ SO(10)
$(1, 1, 0)$	$\mathbb{R}$	4	1	$\phi, \phi, \Sigma, \Sigma^*$
$(1, 1, +1)$	$\mathbb{C}$	2	1	ϕ, Σ
$(1, 1, +2)$	$\mathbb{C}$	1	0	Σ
$(1, 2, +\frac{1}{2})$	$\mathbb{C}$	4	0	Σ, Σ^*, H, H^*
$(1, 3, -1)$	$\mathbb{C}$	1	0	Σ
$(1, 3, 0)$	$\mathbb{R}$	1	0	ϕ
$(3, 2, -\frac{5}{6})$	$\mathbb{C}$	1	1	ϕ
$(3, 2, +\frac{1}{6})$	$\mathbb{C}$	3	1	ϕ, Σ, Σ^*
$(3, 2, +\frac{7}{6})$	$\mathbb{C}$	2	0	Σ, Σ^*
$(3, 3, -\frac{1}{3})$	$\mathbb{C}$	1	0	Σ
$(\bar{3}, 1, -\frac{2}{3})$	$\mathbb{C}$	2	1	ϕ, Σ
$(\bar{3}, 1, +\frac{1}{3})$	$\mathbb{C}$	5	0	$\Sigma, \Sigma, \Sigma^*, H, H^*$
$(\bar{3}, 1, +\frac{4}{3})$	$\mathbb{C}$	1	0	Σ
$(6, 3, +\frac{1}{3})$	$\mathbb{C}$	1	0	Σ
$(\bar{6}, 1, -\frac{4}{3})$	$\mathbb{C}$	1	0	Σ
$(\bar{6}, 1, -\frac{1}{3})$	$\mathbb{C}$	1	0	Σ
$(\bar{6}, 1, +\frac{2}{3})$	$\mathbb{C}$	1	0	Σ
$(8, 1, 0)$	$\mathbb{R}$	1	0	ϕ
$(8, 2, +\frac{1}{2})$	$\mathbb{C}$	2	0	Σ, Σ^*

origin of each copy in terms of SO(10) irreducible representations of scalars labeled as

$$\mathbf{45} \sim \phi_{ij}, \qquad \mathbf{126} \sim \Sigma_{ijklm}, \qquad \mathbf{10}_\mathbb{C} \sim H_i. \qquad (1)$$

In Eq. (1) we wrote the $\mathbf{45}$ as a real antisymmetric matrix, the $\mathbf{126}$ as a complex self-dual antisymmetric five-index tensor, and the $\mathbf{10}_\mathbb{C}$ as a vector with complex components. All Latin indices run from 1 to 10, and are assumed to refer to the real basis of the defining representation $\mathbf{10}$, cf. Appendix A of [34] for more details. The complex conjugates of Σ and H are denoted by Σ^* and H^*, respectively.

Let us note that the main difference between Table I here and an analogous table in [13] is the presence of the complex $\mathbf{10}_\mathbb{C}$, which adds two scalars transforming as $(1, 2, +\frac{1}{2})$ of the SM and two copies of $(\bar{3}, 1, +\frac{1}{3})$. From now on, we shall refer to the representations of this type as SM doublets and triplets.

A. The scalar potential and SO(10) breaking

1. The potential

The tree-level scalar potential of the model in the unbroken phase can be written sector by sector as

$$V_0(\phi, \Sigma, \Sigma^*, H, H^*)$$
$$= V_{45}(\phi) + V_{126}(\Sigma, \Sigma^*) + V_{\text{mix}}(\phi, \Sigma, \Sigma^*)$$
$$+ \tilde{V}_{10}(H, H^*) + \tilde{V}_{\text{mix}}(\phi, \Sigma, \Sigma^*, H, H^*), \qquad (2)$$

where

$$V_{45} = -\frac{\mu^2}{4}(\phi\phi)_0 + \frac{a_0}{4}(\phi\phi)_0(\phi\phi)_0 + \frac{a_2}{4}(\phi\phi)_2(\phi\phi)_2, \quad (3)$$

$$V_{126} = -\frac{\nu^2}{5!}(\Sigma\Sigma^*)_0 + \frac{\lambda_0}{(5!)^2}(\Sigma\Sigma^*)_0(\Sigma\Sigma^*)_0$$
$$+ \frac{\lambda_2}{(4!)^2}(\Sigma\Sigma^*)_2(\Sigma\Sigma^*)_2 + \frac{\lambda_4}{(3!)^2(2!)^2}(\Sigma\Sigma^*)_4(\Sigma\Sigma^*)_4$$
$$+ \frac{\lambda_4'}{(3!)^2}(\Sigma\Sigma^*)_{4'}(\Sigma\Sigma^*)_{4'} + \frac{\eta_2}{(4!)^2}(\Sigma\Sigma)_2(\Sigma\Sigma)_2$$
$$+ \frac{\eta_2^*}{(4!)^2}(\Sigma^*\Sigma^*)_2(\Sigma^*\Sigma^*)_2, \qquad (4)$$

$$V_{\text{mix}} = \frac{i\tau}{4!}(\phi)_2(\Sigma\Sigma^*)_2 + \frac{\alpha}{2 \cdot 5!}(\phi\phi)_0(\Sigma\Sigma^*)_0$$
$$+ \frac{\beta_4}{4 \cdot 3!}(\phi\phi)_4(\Sigma\Sigma^*)_4 + \frac{\beta_4'}{3!}(\phi\phi)_{4'}(\Sigma\Sigma^*)_{4'}$$
$$+ \frac{\gamma_2}{4!}(\phi\phi)_2(\Sigma\Sigma)_2 + \frac{\gamma_2^*}{4!}(\phi\phi)_2(\Sigma^*\Sigma^*)_2, \qquad (5)$$

$$\tilde{V}_{10} = -\xi^2(H^*H)_0 - \xi'^2(HH)_0 - \xi'^{*2}(H^*H^*)_0$$
$$+ h_4(HH)_0(HH)_0 + h_4^*(H^*H^*)_0(H^*H^*)_0$$
$$+ h_3(HH)_0(HH^*)_0 + h_3^*(H^*H^*)_0(H^*H)_0$$
$$+ h_2(H^*H)_0(H^*H)_0 + h_2'(H^*H^*)_0(HH)_0, \qquad (6)$$

$$\tilde{V}_{\text{mix}} = \frac{\kappa_0}{2}(H^*H)_0(\phi\phi)_0 + \kappa_2(H^*H)_2(\phi\phi)_2 + \frac{\kappa_0'}{2}(HH)_0(\phi\phi)_0 + \frac{\kappa_0'^*}{2}(H^*H^*)_0(\phi\phi)_0$$
$$+ \kappa_2'(HH)_2(\phi\phi)_2 + \kappa_2'^*(H^*H^*)_2(\phi\phi)_2 + \frac{\zeta}{4}(\phi\phi)_4(H\Sigma)_4 + \frac{\zeta^*}{4}(\phi\phi)_4(H^*\Sigma^*)_4$$
$$+ \frac{\zeta'}{4}(\phi\phi)_4(H^*\Sigma)_4 + \frac{\zeta'^*}{4}(\phi\phi)_4(H\Sigma^*)_4 + \frac{\rho_0}{5!}(H^*H)_0(\Sigma\Sigma^*)_0 + \frac{\rho_2}{4!}(H^*H)_2(\Sigma\Sigma^*)_2$$
$$+ \frac{\rho_0'}{5!}(HH)_0(\Sigma\Sigma^*)_0 + \frac{\rho_0'^*}{5!}(H^*H^*)_0(\Sigma\Sigma^*)_0 + \frac{\psi_2}{4!}(HH)_2(\Sigma\Sigma)_2 + \frac{\psi_2^*}{4!}(H^*H^*)_2(\Sigma^*\Sigma^*)_2$$
$$+ \frac{\psi_1}{4!}(HH^*)_2(\Sigma\Sigma)_2 + \frac{\psi_1^*}{4!}(H^*H)_2(\Sigma^*\Sigma^*)_2 + \frac{\psi_0}{4!}(H^*H^*)_2(\Sigma\Sigma)_2 + \frac{\psi_0^*}{4!}(HH)_2(\Sigma^*\Sigma^*)_2$$
$$+ i\tau'(\phi)_2(HH^*)_2 + \frac{\varphi}{3!}(H\Sigma)_4(\Sigma\Sigma^*)_4 + \frac{\varphi^*}{3!}(H^*\Sigma^*)_4(\Sigma\Sigma^*)_4 + \frac{\varphi'}{3!}(H^*\Sigma)_4(\Sigma\Sigma^*)_4 + \frac{\varphi'^*}{3!}(H\Sigma^*)_4(\Sigma\Sigma^*)_4. \qquad (7)$$

Note that the definitions of the "old" parts of the potential corresponding solely to the **126** ⊕ **45** sector are identical to those entertained in [13], while the new parts involving the **10**$_{\text{C}}$ are denoted by a tilde.

To avoid any confusion, we explicitly wrote complex conjugate terms where applicable. The notation for contractions is a straightforward extension of the one already specified in [13]: the subscript of an object in parentheses indicates the number of uncontracted indices (placed symmetrically at the end of each factor), e.g.,[1]

$$(H^*H)_0 \equiv H_i^*H_i, \qquad (H^*H)_2 \equiv H_i^*H_j, \qquad (8)$$

$$(H\Sigma)_4 \equiv H_m\Sigma_{mijkl}, \qquad (\Sigma\Sigma^*)_0 \equiv \Sigma_{ijklm}\Sigma_{ijklm}^*, \qquad (9)$$

---

[1]Note that four-index objects have two possible contractions, namely, $(X)_4(Y)_4 \equiv X_{ijkl}Y_{ijkl}$ and $(X)_{4'}(Y)_{4'} \equiv X_{ijkl}Y_{ikjl}$.

$$(\Sigma\Sigma^*)_2 \equiv (\Sigma\Sigma^*)_{mn} = \Sigma_{ijklm}\Sigma_{ijkln}^*, \qquad (10)$$

$$(\Sigma\Sigma^*)_4 \equiv (\Sigma\Sigma^*)_{lmno} = \Sigma_{ijklm}\Sigma_{ijkno}^*. \qquad (11)$$

As a cross-check for the completeness of the scalar potential, we confirmed that all invariants in Eqs. (3)–(7) are linearly independent, while their number matches the counting by the standard Hilbert series methods [35,36] [assisted by the *Mathematica* package LieART 2.0 [37,38], which provided the weight vectors for the SO(10) representations].

In total, the list of dimensionless parameters in the scalar potential now consists of 15 real and 14 complex couplings, from which 6 and 12 are new compared to the Higgs model [13], respectively. For further convenience we list all couplings, both dimensionless and dimensionful, in Table II.

TABLE II. The parameters of the scalar potential of Eq. (2) arranged according to their novelty (i.e., whether they have already been present in [13] or not), reality/complexity ($\mathbb{R}/\mathbb{C}$) and their mass dimension D.

	$D = 0$	$D = 1$	$D = 2$
Old $\mathbb{R}$	$a_0, a_2, \lambda_0, \lambda_2, \lambda_4, \lambda_4', \alpha, \beta_4, \beta_4'$	τ	μ^2, ν^2
New $\mathbb{R}$	$h_2, h_2', \kappa_0, \kappa_2, \rho_0, \rho_2$	τ'	ξ^2
Old $\mathbb{C}$	γ_2, η_2		
New $\mathbb{C}$	$h_4, h_3, \kappa_0', \kappa_2', \zeta, \zeta', \rho_0', \psi_2, \psi_1, \psi_0, \varphi, \varphi'$		ξ'^2

2. Symmetry breaking

Let us now turn to the spontaneous symmetry breaking (SSB) of the GUT symmetry. The scalar sector contains two real SM singlets in the **45** and one complex SM singlet in the **126**, with no extra SM singlets in the added **10**$_\mathbb{C}$. The SSB thus proceeds identically as in the pure Higgs model [13].

In short, the SM singlet fields obtain nonzero vacuum expectation values (VEVs) defined as

$$\langle (1, 1, 1, 0)_{45} \rangle \equiv \sqrt{3}\omega_{BL},$$
$$\langle (1, 1, 3, 0)_{45} \rangle \equiv \sqrt{2}\omega_R,$$
$$\langle (1, 1, 3, +2)_{126} \rangle \equiv \sqrt{2}\sigma, \qquad (12)$$

where the numbers in parentheses refer to their $SU(3)_c \times SU(2)_L \times SU(2)_R \times U(1)_{B-L}$ transformation properties and the subscripts 45 and 126 denote their SO(10) origin. The redefinition of the overall phase of Σ can make σ real and positive, while a sign redefinition of ϕ allows one to choose ω_R positive.

It is convenient to define the dimensionless universal VEV ratio

$$\chi := \frac{\omega_{BL}\omega_R}{|\sigma|^2}, \qquad (13)$$

which is a quantity that appears in the solution of the stationarity conditions for the SM vacuum, as well as in loop corrections to the effective one-loop scalar masses. Perturbativity requires $|\chi| \lesssim 1$, thus greatly constraining the set of viable breaking patterns, see [13]. As mentioned in the Introduction, we focus only on the regime $|\omega_{BL}| \ll |\sigma| \ll |\omega_R|$ (to be referred to as $\omega_{BL} \to 0$) featuring the $SU(4)_C \times SU(2)_L \times U(1)_R$ intermediate symmetry, abbreviated as G_{421}, which turns out to be much more promising than any of the other options, see [13].

The large hierarchy between the VEVs in Eq. (12) allows us to imagine the SSB as a two stage process:

$$SO(10)$$
$$\downarrow \omega_R$$
$$SU(4)_C \times SU(2)_L \times U(1)_R$$
$$\downarrow \sigma$$
$$SU(3)_c \times SU(2)_L \times U(1)_Y,$$

where, phenomenologically, ω_R is the GUT-breaking scale and σ plays the role of the seesaw scale for neutrinos. The ω_{BL} VEV is irrelevant for the symmetry breaking here and obtains only an induced value $\omega_{BL} = \chi|\sigma|^2/\omega_R$.

The dimensionful parameters $\{\mu, \nu, \tau\}$ are related to the $\{\omega_{BL}, \omega_R, \sigma\}$ VEVs via the vacuum stationarity conditions, which take the tree-level form

$$\mu^2 = (8a_0 + 2a_2)\omega_R^2 + 2(a_2\chi + 2\alpha + 2\beta_4')|\sigma|^2, \qquad (14)$$

$$\nu^2 = 2(\alpha + 3\beta_4' + a_2\chi)\omega_R^2 + (4\lambda_0 + 12\beta_4'\chi + 5a_2\chi^2)|\sigma|^2, \qquad (15)$$

$$\tau = (4\beta_4' + a_2\chi)\omega_R, \qquad (16)$$

where $O(\frac{\omega_{BL}}{\omega_R})$ terms were neglected in the $\omega_{BL} \to 0$ regime.

One can thus consider the VEVs ω_R and σ, along with the ratio χ, to be the input parameters, and take the $\{\mu, \nu, \tau\}$ parameter values computed from the vacuum conditions, as in [13]. Note that with the addition of the **10**$_\mathbb{C}$, new mass scales are introduced through the $\{\xi, \xi', \tau'\}$ parameters. Since, at the tree level, these influence only the doublets and triplets (see Sec. II A 3), the aforementioned interpretation of ω_R and σ can be retained, assuming that none of the new dimensionful parameters is parametrically larger than ω_R.

3. The tree-level mass spectrum

Since there are no GUT or intermediate-scale VEVs in the newly introduced **10**$_\mathbb{C}$, all new couplings in Table II impact only those tree-level scalar-mass matrices, which include a state from **10**$_\mathbb{C}$. Consequently, almost all scalar mass matrices of the **45** $\oplus$ **126** $\oplus$ **10**$_\mathbb{C}$ model at stake are identical to those of the **45** $\oplus$ **126** Higgs model [13], with the only exceptions of the SM doublets $(1, 2, +\frac{1}{2})$ and triplets $(\bar{3}, 1, +\frac{1}{3})$. Similarly, the gauge boson masses are identical in these two cases as well.

For those tree-level mass matrices that are common to both scenarios, the interested reader is referred to [2,8] (with minor corrections included in the latter); their approximate forms in the $\omega_{BL} \to 0$ limit are given in [13]. The enlarged matrices for doublets and triplets, in which the vacuum of Eqs. (14)–(16) has been inserted (and only the dominant contributions in the $\omega_{BL} \to 0$ regime were retained), read

$$M^2\left(1,2,+\tfrac{1}{2}\right)_{\text{tree}} = \begin{pmatrix} \left(\tfrac{\beta_4}{2}-9\beta'_4-3a_2\chi\right)\omega_R^2 & -2\gamma_2\omega_R^2 & -\sqrt{6}\zeta'\chi|\sigma|^2 & -\sqrt{6}\zeta\chi|\sigma|^2 \\ -2\gamma_2^*\omega_R^2 & \left(\tfrac{\beta_4}{2}-\beta'_4-a_2\chi\right)\omega_R^2 & \sqrt{6}(16\phi^*+\zeta^*\chi)|\sigma|^2 & \sqrt{6}(16\phi'^*+\zeta'^*\chi)|\sigma|^2 \\ -\sqrt{6}\zeta'^*\chi|\sigma|^2 & \sqrt{6}(16\phi+\zeta\chi)|\sigma|^2 & -\xi^2-\tfrac{\tau'\omega_R}{24}+(2\kappa_0+\kappa_2)\omega_R^2 & -2\xi'^2+2(2\kappa'_0+\kappa'_2)\omega_R^2 \\ -\sqrt{6}\zeta^*\chi|\sigma|^2 & \sqrt{6}(16\phi'+\zeta'\chi)|\sigma|^2 & -2\xi'^{2*}+2(2\kappa'^*_0+\kappa'^*_2)\omega_R^2 & -\xi^2+\tfrac{\tau'\omega_R}{24}+(2\kappa_0+\kappa_2)\omega_R^2 \end{pmatrix},$$

$$(17)$$

$$M^2\left(\bar{3},1,+\tfrac{1}{3}\right)_{\text{tree}} = \begin{pmatrix} (\beta_4-4\beta'_4-2a_2\chi)\omega_R^2 & 4\gamma_2\omega_R^2 & 2\sqrt{2}(\beta_4\chi-8\lambda'_4)|\sigma|^2 & -\sqrt{2}\zeta\omega_R^2 & -\sqrt{2}\zeta'\omega_R^2 \\ 4\gamma_2^*\omega_R^2 & (\beta_4-4\beta'_4-2a_2\chi)\omega_R^2 & 0 & -\sqrt{2}\zeta'^*\omega_R^2 & -\sqrt{2}\zeta^*\omega_R^2 \\ 2\sqrt{2}(\beta_4\chi-8\lambda'_4)|\sigma|^2 & 0 & (2\beta_4-4\beta'_4-2a_2\chi)\omega_R^2 & -4(8\varphi+\zeta\chi)|\sigma|^2 & -4(8\varphi'+\zeta'\chi)|\sigma|^2 \\ -\sqrt{2}\zeta^*\omega_R^2 & -\sqrt{2}\zeta'\omega_R^2 & -4(8\varphi^*+\zeta^*\chi)|\sigma|^2 & -\xi^2+2\kappa_0\omega_R^2 & -2\xi'^{2*}+4\kappa'^*_0\omega_R^2 \\ -\sqrt{2}\zeta'^*\omega_R^2 & -\sqrt{2}\zeta\omega_R^2 & -4(8\varphi'^*+\zeta'^*\chi)|\sigma|^2 & -2\xi'^2+4\kappa'_0\omega_R^2 & -\xi^2+2\kappa_0\omega_R^2 \end{pmatrix},$$

$$(18)$$

where the basis of the row states is defined as follows:

for $\left(1,2,+\tfrac{1}{2}\right):\left\{\left(15,2,+\tfrac{1}{2}\right)_\Sigma,\left(15,2,-\tfrac{1}{2}\right)^*_{\Sigma^*},\right.$

$$\left.\times\left(1,2,+\tfrac{1}{2}\right)_H,\left(1,2,-\tfrac{1}{2}\right)^*_{H^*}\right\},\quad(19)$$

for $\left(\bar{3},1,+\tfrac{1}{3}\right):\{(6,1,0)_\Sigma,(6,1,0)^*_{\Sigma^*},(\overline{10},1,0)_\Sigma,$

$$\times(6,1,0)_H,(6,1,0)^*_{H^*}\}.\quad(20)$$

The basis states are unambiguously specified by their intermediate $SU(4)_C\times SU(2)_L\times U(1)_R$ and GUT symmetry origin in the parentheses and in the subscripts, respectively; their ordering is consistent with the one suggested by Table I. The basis for column states is conjugate to that of the basis for rows.

Note that in this basis the upper-left 2×2 block of Eq. (17) and the upper-left 3×3 block of Eq. (18) depend only on the old couplings. These sub-blocks are identical to the Higgs model expressions [13], while all other entries (the enlarged part) involve only the new couplings. Furthermore, in the limit[2] $\sigma\to0$ one recovers the intermediate G_{421} symmetry with the mixing occurring solely between the same type of representations within the bases of Eqs. (19) and (20). In particular, the doublet mass matrix becomes block diagonal in this limit.

The tree-level spectrum, however, is qualitatively not the end of the story in the model under consideration. A key observation was made in [24,25] that certain scalar states

cannot be made simultaneously nontachyonic at tree-level unless the breaking proceeds through an intermediate (flipped) SU(5) symmetry. The problematic states include the SM triplet (1, 3, 0) and octet (8, 1, 0), along with the singlet (1, 1, 0) as pointed out in [8]. Given their specific behavior in various limits, these states were dubbed the pseudo-Goldstone bosons (PGBs), and we shall refer to them as such from now on.

It is very instructive to consider the PGBs in the strict $\omega_{BL}\to0$ regime. In such a case the field $(\bar{3},1,-\tfrac{2}{3})$, sharing the same parent (15, 1, 0) multiplet of G_{421} with (8, 1, 0) and (1, 1, 0), also joins the list of states whose masses acquire a particularly simple form. Taking the limit $\sigma\to0$, we find the dominant parts of the tree-level masses of these fields to be

$$M_S^2(1,3,0) = 4a_2\omega_R^2,\quad(21)$$

$$M_S^2(8,1,0) = -2a_2\omega_R^2,\quad(22)$$

$$M_S^2(1,1,0)_3 = -2a_2\omega_R^2,\quad(23)$$

$$M_S^2\left(\bar{3},1,-\tfrac{2}{3}\right)_2 = -2a_2\omega_R^2.\quad(24)$$

Note that subscripts are used when multiple states with the same G_{321} quantum numbers are present, and they label the relevant mass eigenstates in an ascending mass order. Observe also that no choice of a_2 (except for the singular $a_2=0$ case) can make all these states simultaneously nontachyonic.

Remarkably, this situation can be remedied by loop corrections (as first discussed in [1]) if one takes $|a_2|\ll1$, so that the tree-level PGB masses become suppressed.

---

[2]Note that the $\sigma\to0$ limit is properly taken by keeping the universal ratio χ in Eq. (13) fixed.

However, this also means that any in-depth analysis of the model requires access to the one-loop scalar spectrum; for that sake the numerical methods developed for the $\mathbf{45} \oplus \mathbf{126}$ Higgs model in [13] have been extended to the $\mathbf{45} \oplus \mathbf{126} \oplus \mathbf{10}_{\mathbb{C}}$ case.

B. The Yukawa sector

1. General considerations

With both the $\mathbf{126}$ and $\mathbf{10}_{\mathbb{C}}$ at play, the renormalizable Yukawa Lagrangian consists schematically of the terms [39] [with the SO(10) indices and Lorentz structures suppressed]

$$\mathcal{L}_Y = \mathbf{16}_F^a (Y_{10}^{ab} \mathbf{10}_{\mathbb{C}} + \tilde{Y}_{10}^{ab} \mathbf{10}_{\mathbb{C}}^* + Y_{126}^{ab} \mathbf{126}^*) \mathbf{16}_F^b + \text{H.c.}, \quad (25)$$

where $\mathbf{16}_F^a$ contains fermions, $a, b = 1, \ldots, 3$ denote family indices, and the matrices Y_{10}, $\tilde{Y}_{10}$, and Y_{126} are complex symmetric 3×3 matrices in family space.

The electrically neutral components of the SM weak doublets with hypercharges $\pm 1/2$ acquire VEVs in the electroweak broken phase. They are labeled by

$$v_{10}^u = \left\langle \left(1, 2, +\frac{1}{2}\right)_{10} \right\rangle,$$

$$v_{10}^d = \left\langle \left(1, 2, -\frac{1}{2}\right)_{10} \right\rangle,$$

$$v_{126}^u = \left\langle \left(1, 2, +\frac{1}{2}\right)_{\overline{126}} \right\rangle,$$

$$v_{126}^d = \left\langle \left(1, 2, -\frac{1}{2}\right)_{\overline{126}} \right\rangle. \quad (26)$$

The notation above is straightforward: the subscripts denote their SO(10) origin and their superscripts u and d indicate the $+1/2$ and $-1/2$ hypercharges, respectively. The tree-level (GUT-scale) quark and lepton mass matrices then take the following form:

$$M_U = Y_{10} v_{10}^u + \tilde{Y}_{10} v_{10}^{d*} + Y_{126} v_{126}^u, \quad (27)$$

$$M_D = Y_{10} v_{10}^d + \tilde{Y}_{10} v_{10}^{u*} + Y_{126} v_{126}^d, \quad (28)$$

$$M_E = Y_{10} v_{10}^d + \tilde{Y}_{10} v_{10}^{u*} - 3 Y_{126} v_{126}^d, \quad (29)$$

$$M_\nu^D = Y_{10} v_{10}^u + \tilde{Y}_{10} v_{10}^{d*} - 3 Y_{126} v_{126}^u, \quad (30)$$

where U, D, and E refer, respectively, to the up, down, and charged lepton sectors, while M_ν^D is the Dirac type neutrino mass matrix. The EW VEVs are normalized such that

$$v_{\text{SM}}^2 = |v_{10}^u|^2 + |v_{10}^d|^2 + |v_{126}^u|^2 + |v_{126}^d|^2, \quad (31)$$

where $v_{\text{SM}} \doteq 174$ GeV. Furthermore, the seesaw type I and II Majorana mass matrices read

$$M_\nu^{M,\text{type I}} \propto Y_{126} \sigma, \qquad M_\nu^{M,\text{type II}} \propto Y_{126} w, \quad (32)$$

where

$$w = \langle (1, 3, +1)_{\overline{126}} \rangle \quad (33)$$

is the induced EW VEV of the scalar $SU(2)_L$ triplet relevant for the type II seesaw.

Renormalizable Yukawa sectors of SO(10) GUTs have been studied in great detail in the literature, see, e.g., [6,39–51]. Let us just summarize the salient points below:

(1) Due to the SO(10) decomposition $\mathbf{16} \otimes \mathbf{16} = \mathbf{10} \oplus \mathbf{120} \oplus \mathbf{126}$ [52], the most general renormalizable Yukawa sector includes scalar representations $\mathbf{126}$, $\mathbf{10}$, and/or $\mathbf{120}$, with the latter requiring an anti-symmetric Yukawa matrix. Since at least two Yukawa matrices are required for a successful fit of fermion masses and mixing, the Higgs model $\mathbf{45} \oplus \mathbf{126}$ requires an upgrade to become potentially realistic; the addition of an extra $\mathbf{10}$ represents the obvious option here.[3]

(2) The added $\mathbf{10}$ should better be complex (or equivalently, two copies of a real $\mathbf{10}$ should be considered), otherwise the relation $v_{10}^u = v_{10}^{d\,*}$ among the SM VEV projections emerges, and the fit of SM fermion masses and mixing is not possible, since it clashes with the phenomenological requirement [39]

$$\left| \frac{v_{10}^u}{v_{10}^d} \right| \approx \frac{m_t}{m_b} \gg 1. \quad (34)$$

(3) Two different Yukawa terms can be constructed with the complex $\mathbf{10}_{\mathbb{C}}$ (in the non-SUSY case), so the resulting theory has three Yukawa matrices in total and a good fermion-sector fit is easily attained. In fact, such a fit is already possible with a single Yukawa matrix associated to a real $\mathbf{10}$ along with the one associated to $\mathbf{126}$, which is a scenario arising in the SUSY case [53,54] or if a Peccei-Quinn-like (PQ) global U(1) symmetry is introduced [39–47]. In the latter case the typical assignment of the PQ charges reads

$$[\mathbf{16}_F]_{PQ} = +1, \qquad [\mathbf{45}]_{PQ} = 0,$$
$$[\mathbf{126}]_{PQ} = +2, \qquad [\mathbf{10}]_{PQ} = -2. \quad (35)$$

---

[3]The extension with an additional $\mathbf{10}$ is clearly minimal in terms of extra degrees of freedom, but it also has the advantage of the symmetry of the corresponding Yukawa matrices. The antisymmetric Yukawa of the $\mathbf{120}$ with only one more symmetric Yukawa matrix of the $\mathbf{126}$ does not lead to realistic fermion mass matrices [41].

These charges forbid the $\tilde{Y}_{10}$ Yukawa coupling in Eq. (25), thus increasing the predictivity of the fit. Furthermore, the PQ symmetry forbids a number of couplings in the scalar potential (2)–(7) which, naively, may look as a good way to greatly simplify the current analysis. Unfortunately, any nontrivial assignment of the PQ charge to Σ necessarily forbids the same γ_2 term in Eq. (4) that was found to be necessary for curing the tachyonicity of PGB states in the Higgs model $\mathbf{45} \oplus \mathbf{126}$, cf. [13], so we shall not entertain this option at all.

(4) A successful fermion mass fit accomplished via the tree-level relations of Eqs. (27)–(30) requires a significant admixture of the weak doublets from both $\mathbf{10}_\mathbb{C}$ and $\mathbf{126}$ within the SM Higgs doublet, otherwise either $v_{126}^{u,d} \approx 0$ or $v_{10}^{u,d} \approx 0$, for which the Yukawa fit does not work.[4]

2. The structure of the doublet mass matrix

The last point above has very important ramifications for the structure of the doublet mass matrix of Eq. (17). In the basis of Eq. (19) it can be schematically written as

$$M^2\left(1, 2, +\frac{1}{2}\right) = \begin{pmatrix} M_{126}^2 & M_{\text{mix}}^2 \\ M_{\text{mix}}^{2\dagger} & M_{10}^2 \end{pmatrix}, \qquad (36)$$

where the 2×2 block structures M_{126}^2, M_{10}^2, and M_{mix}^2 encompass contributions of different SO(10) origin. To this end, the former two mix doublets solely within the $\mathbf{126}$ and $\mathbf{10}_\mathbb{C}$, respectively, while the last one controls their crosstalk. Since no mixing among the $\mathbf{126}$ and $\mathbf{10}_\mathbb{C}$ is possible until the intermediate G_{421} symmetry gets broken, the M_{mix}^2 block must vanish for $\sigma \to 0$. Furthermore, the expected magnitudes of entries in the M_{126}^2 and M_{10}^2 blocks are $\mathcal{O}(\omega_R^2)$ while M_{mix}^2 is expected at the $|\sigma|^2$ level,[5] with $|\sigma|^2 \ll \omega_R^2$ assumed. This should be the case at all perturbative orders, and can be explicitly verified for the tree-level expression in Eq. (17).

The requirement of accommodating the SM Higgs doublet implies that one eigenvalue of the matrix in Eq. (36) should be fine-tuned to about $(125\ \text{GeV})^2$. On top of that, the doublet-admixture condition of Sec. II B requires the SM Higgs doublet to have a sufficiently large projection to both the $\mathbf{126}$ and $\mathbf{10}_\mathbb{C}$ sectors. Since, however, M_{mix}^2 is of the order of $|\sigma|^2$, this boils down to a need for an

initial pretuning of at least one eigenvalue in both M_{126}^2 and M_{10}^2 from their natural scale of ω_R^2 down to roughly $|\sigma|^2$.

The pretuning requirement can be brought into sharper quantitative form by estimating the required weight of the **126**-components within the SM Higgs. The corresponding VEV ratio obeys

$$\sqrt{\frac{|v_{126}^u|^2 + |v_{126}^d|^2}{v_{\text{SM}}^2}} = \frac{1}{4}\frac{|\text{Tr}M_D - \text{Tr}M_E|}{v_{\text{SM}}}\frac{\sqrt{1 + |r|^2|s|^2}}{|\text{Tr}Y_{126}|}$$
$$\gtrsim \frac{|\text{Tr}M_D - \text{Tr}M_E|}{v_{\text{SM}}}\frac{\sqrt{1 + |r|^2|s|^2}}{4}, \quad (37)$$

where M_D and M_E are defined in Eqs. (28) and (29), r and s stand for the usual ratios [46]

$$r := \frac{v_{10}^u}{v_{10}^d}, \qquad s := \frac{v_{126}^u}{v_{126}^d}\frac{v_{10}^d}{v_{10}^u}, \qquad (38)$$

and perturbativity has been assumed for Y_{126} in the form of $\text{Tr}[Y_{126}] \lesssim 1$. Inspecting the existing Yukawa sector fits like [46], one obtains a conservative estimate[6]

$$\sqrt{\frac{|v_{126}^u|^2 + |v_{126}^d|^2}{v_{\text{SM}}^2}} \gtrsim 3 \times 10^{-2} \equiv \epsilon. \qquad (39)$$

In terms of the eigenvalues of the two diagonal blocks (denoted by $m_{126\pm}^2$ for M_{126}^2 and $m_{10\pm}^2$ for M_{10}^2, with $+$ referring to the larger and $-$ to the smaller ones), the pretuning conditions can be recast as

$$m_{10-}^2 \sim |\sigma|^2, \qquad m_{126-}^2 \sim |\sigma|^2/\epsilon, \qquad (40)$$

with $\epsilon = 3 \times 10^{-2}$. For better numerical intuition, the $\mathbf{45} \oplus \mathbf{126}$ Higgs model analysis [13] suggests $\omega_R \gtrsim 10^{14.8}$ GeV and $|\sigma| < 10^{11.8}$ GeV, and hence $|\sigma|^2 \lesssim 10^{-6}\omega_R^2$, which translates the conditions in Eq. (40) into[7]

---

[4]Note that the case $v_{126}^{u,d} \approx 0$ implies a (GUT-scale) SU(5)-like relation $M_D \approx M_E$, while the case $v_{10}^{u,d} \approx 0$ yields $M_D \approx -3M_E$, none of which is realistic.

[5]There can be no $\sigma\omega_R$ contribution in M_{mix}^2 due to gauge symmetry. This can be seen by considering the $\text{SU}(4)_C$ factor, under which the doublet/antidoublet product transforms as a 15-plet, while $\sigma \sim \overline{10}$ and $\omega_R \sim 1$.

[6]Taken strictly, the fermion fit in [46] assumes a PQ-like setting with only two Yukawa matrices, but it is still to a large degree applicable to Eq. (37) in the more general three Yukawa case. Namely, the size of $M_D - M_E$ is enforced by the difference $y_b - y_\tau$ at the GUT scale (unrelated to $\tilde{Y}_{10}$), while only a large $|rs|$ can simultaneously achieve a suitably large M_U (large top Yukawa) and a small M_D^D. Note that the seesaw scale $|\sigma| \sim 10^{11}$ GeV is rather small in the current case, therefore within type I seesaw a small M_ν^D is indeed needed to suppress the enhanced inverse of $M_\nu^{M,\text{type I}}$ for suitable neutrino masses.

[7]Note that in [13] the estimates for ω_R and $|\sigma|$ have been obtained in a simplified setting without $\mathbf{10}_\mathbb{C}$; however, since these follow from the unification analysis where the presence/absence of the extra $\mathbf{10}_\mathbb{C}$ plays a marginal role, one can expect very similar constraints to be relevant also for the full-model case, see Appendix A.

$$m_{10-}^2 \sim 10^{-6}\omega_R^2, \qquad m_{126-}^2 \sim 3.3 \times 10^{-5}\omega_R^2. \quad (41)$$

The M_{10}^2 block is the only part of the tree-level scalar spectrum that depends on the new couplings κ_0', κ_2', and τ'. The pretuning of m_{10-}^2 is thus easily achieved via these parameters.

On the other hand, it is namely the condition on m_{126-}^2 in Eq. (40) that turns out to be difficult to conform to in the potentially realistic and perturbative parts of the model parameter space, thus heavily disfavoring the **45 $\oplus$ 126 $\oplus$ 10$_{\mathbb{C}}$** setting as a basis for a robust and calculable GUT scenario. This pretuning issue is demonstrated in Sec. III at tree-level analytically, and then in Sec. IV at one-loop level numerically.

To summarize, the arrangement of a SM-compatible Higgs doublet mass in the $M^2(1, 2, +\frac{1}{2})$ mass matrix first requires a pretuning to the intermediate scale in each of the M_{126}^2 and M_{10}^2 blocks, before the full fine-tuning down to the EW scale should be performed. This procedure brings in an additional set of constraints on the scalar potential parameters. The obstructions to pretuning in the **126** sector and the associated implications are the main focus of the remainder of this study.

III. DOUBLET FINE-TUNING AT TREE LEVEL—ANALYTICALLY

It is instructive to first consider the pretuning obstruction for doublets in M_{126}^2 of Eq. (36) at tree level, since one has analytic grip on the tree-level mass expressions, see Eq. (17). A possible reservation of the reader may be that the model's first consistent perturbative order is only at one loop, but note that these intricacies are intimately connected only to the PGB sector of scalars. Quantitatively, the quantum corrections thus play no bigger role in the non-PGB sectors, e.g., in the doublet sector, than in the usual perturbative situation with a consistent tree order. A tree-level consideration of doublets will thus offer valuable insight, while the quantum nature of the model will percolate into the analysis only through limitations on the parameter space, as will become apparent in due course.

The tree-level eigenvalues $m_{126\pm,(0)}^2$ of the M_{126}^2 block are

$$m_{126\pm,(0)}^2 = \left(\frac{\beta_4}{2} - 5\beta_4' - 2a_2\chi \pm \sqrt{(4\beta_4' + a_2\chi)^2 + 4|\gamma_2|^2}\right)\omega_R^2, \quad (42)$$

where only the dominant contributions are considered given the VEV hierarchy $|\sigma| \ll |\omega_R|$. Doublet pretuning demands that $m_{126-,(0)}^2$ is brought down roughly to $|\sigma|^2/\epsilon$, cf. Eq. (40).

The pretuning of $m_{126-,(0)}^2$ is most conveniently viewed as a constraint on $|\gamma_2|$, since this parameter is present at tree-level only in the mass expressions for multiplets $(15, 2, +\frac{1}{2})$ and $(6, 1, 0)$ of the G_{421} intermediate symmetry,

to which the SM doublets $(1, 2, +\frac{1}{2})$ and triplets $(\bar{3}, 1, +\frac{1}{3})$, respectively, belong, cf. Tables VII and IX in [13]. Consequently, the constraint on $|\gamma_2|$ is directly entangled only with the nontachyonicity of triplets, which thus warrants special attention.

Nontachyonicity of the SM triplets requires the mass-square matrix in Eq. (18) to be positive (semi)definite. Applying Sylvester's criterion for positive-definiteness requires the leading principal minors (the determinants of the 1×1, 2×2, etc. upper-left submatrices) of $M^2(\bar{3}, 1, +\frac{1}{3})_{\text{tree}}$ to be positive. The relevant constraints are already given by the first three minors, which involve the triplet states from the representation **126** only:

$$0 < \mathcal{M}_{1\times1}^2 = (\beta_4 - 4\beta_4' - 2a_2\chi)\omega_R^2, \quad (43)$$

$$0 < \mathcal{M}_{2\times2}^2 = \theta\omega_R^4, \quad (44)$$

$$0 < \mathcal{M}_{3\times3}^2 = \theta(\beta_4 - 4\beta_4' - 2a_2\chi)\omega_R^6 + \mathcal{O}(|\sigma|^2\omega_R^2), \quad (45)$$

where the entire γ_2 dependence is conveniently packaged into a single parameter θ defined by

$$\theta \equiv (\beta_4 - 4\beta_4' - 2a_2\chi)^2 - 16|\gamma_2|^2. \quad (46)$$

The triplet nontachyonicity conditions in Eqs. (43)–(45) (allowing now for the semidefinite case) simplify to

$$\theta \geq 0, \qquad \beta_4 - 4\beta_4' - 2a_2\chi \geq 0, \quad (47)$$

and these need to be amended by the nontachyonicity requirements from all other non-PGB scalar fields at tree-level (cf. Table IX in [13]):

$$4\beta_4' + a_2\chi \leq 0,$$
$$2\beta_4' + a_2\chi \leq 0,$$
$$\beta_4 - 2\beta_4' - a_2\chi \geq 0,$$
$$\beta_4 - 10\beta_4' - 4a_2\chi \geq 0. \quad (48)$$

Furthermore, the comprehensive analysis of the **45 $\oplus$ 126** SO(10) Higgs model in [13] gives the viable ranges for these parameters:

$$\beta_4 \in [0.2, 1], \qquad \beta_4' \in [-0.2, -0.01],$$
$$a_2 \in [-0.05, 0.05], \qquad \chi \in [-1, 1]. \quad (49)$$

The viable region must therefore lie in the multidimensional box defined by Eq. (49). Note that restricting to this box is precisely where the necessary requirements for PGB nontachyonicity (at one-loop level) have slipped in. Interestingly, the ranges of Eq. (49) make all inequalities in Eq. (48) except for the second one redundant.

We now return to the quantity $m^2_{126-,(0)}$ that we wish to tune, and rewrite it in terms of θ instead of $|\gamma_2|$:

$$m^2_{126-,(0)}(\theta) = \left(\frac{\beta_4}{2} - 5\beta'_4 - 2a_2\chi - \frac{1}{2}\sqrt{4(4\beta'_4 + a_2\chi)^2 + (\beta_4 - 4\beta'_4 - 2a_2\chi)^2 - \theta} \right)\omega^2_R. \tag{50}$$

Notice that $m^2_{126-,(0)}(\theta)$ is an increasing function of θ, i.e.,

$$\frac{\partial m^2_{126-,(0)}}{\partial \theta} = \frac{1}{4}\frac{\omega^2_R}{\sqrt{4(4\beta'_4 + a_2\chi)^2 + (\beta_4 - 4\beta'_4 - 2a_2\chi)^2 - \theta}} > 0. \tag{51}$$

Triplet nontachyonicity in Eq. (47) requires a non-negative θ, and thus

$$m^2_{126-,(0)}(\theta) \geq m^2_{126-,(0)}(0) = \left(\frac{\beta_4}{2} - 5\beta'_4 - 2a_2\chi - \frac{1}{2}\sqrt{4(4\beta'_4 + a_2\chi)^2 + (\beta_4 - 4\beta'_4 - 2a_2\chi)^2} \right)\omega^2_R \tag{52}$$

for any fixed choice of β_4, β'_4, and $a_2\chi$. As a numerical exercise, we can then find the lowest numerical value for $m^2_{126-,(0)}$ at $\theta = 0$ given the parameter restrictions of Eq. (47)–(49):

$$\min_{\beta_4,\beta'_4,a_2\chi} [m^2_{126-,(0)}(0)] \gtrsim 0.008\omega^2_R, \tag{53}$$

which is obtained for $\beta_4 = 0.2$, $\beta'_4 = -0.01$, $a_2\chi = 0.02$. Comparing with the requirement of Eq. (41), we see that doublet pretuning cannot be directly achieved at tree level.

Incidentally, solving $\theta = 0$ for the minimal point gives $|\gamma_2| = 0.05$, which is smaller than the rough lower bound $|\gamma_2| \gtrsim 0.1$ from [13], indicating the estimate in Eq. (53) to actually be conservative and making the fine-tuning situation worse. An attainable value is, e.g., for $(\beta_4, \beta'_4, a_2\chi, |\gamma_2|) = (0.4, -0.01, 0.02, 0.1)$:

$$m^2_{126-} \approx 0.009\omega^2_R. \tag{54}$$

To summarize, we demonstrated at tree level that doublet pretuning in the **126**-block is obstructed by the nontachyonicity constraints of other scalars. This, however, does not conclude the analysis; the tree-level value in Eq. (54) is sufficiently suppressed that quantum corrections (shown to be easily at 10% of ω^2_R or larger in Sec. IV) may bridge the pretuning gap, provided they properly align for the doublets and the obstruction states.

Ironically, the burden of making the model realistic is thus again placed on quantum corrections, as it was for attaining a suitable vacuum. We show in the next section that the obstruction to doublet pretuning is instead significantly reinforced at one-loop level, leading to bleak prospects for the model.

IV. DOUBLET FINE-TUNING AT ONE LOOP—NUMERICALLY

In the tree-level analysis of Sec. III it was made clear that a successful pretuning in the **126**-sector may happen only if loop-corrections to various fields properly align. To assess the feasibility of such a situation, a complete one-loop analysis along the lines of [13] is required for the full model. The usual perturbativity and nontachyonicity constraints are, however, to be amended by the pretuning requirements.

Such an analysis involves numeric scans of the parameter space, for which at every considered point the tree-level and one-loop scalar spectrum is computed. The one-loop calculation is performed by numerically evaluating the one-loop regularized effective mass squares.[8]

The one-loop analysis in this section is organized as follows: the technical requirements of pretuning in the context of perturbation theory are discussed and formulated in Sec. IV A, the necessary criteria for a parameter point to be considered viable are summarized in Sec. IV B, the parameter inputs of the analysis are listed in Sec. IV C, and the results of the parameter space scans are presented in Sec. IV D.

A. Fine-tuning of doublets in perturbation theory

The block structure of the doublet mass matrix in Eq. (36) and the required level of pretuning in Eq. (40) as described in Sec. II B 2 refer to quantities that would ideally be computed to all orders in perturbation theory (with an optimal truncation due to the asymptotic nature of this series). In practice, however, one only has access to the

---

[8]The regularized effective scalar mass is the scalar mass computed from the one-loop effective potential in which IR diverging logarithmic contributions are tamed by mimicking the shift from the effective to the physical mass. The associated techniques are given in [13].

few lowest orders, while the effect of higher-order corrections, despite not being readily accessible, should nonetheless be anticipated. The goal of the discussion below is to formulate a technical criterion for the desired pretuning in the **126** sector in the context of perturbation theory.

In Sec. II B 2 the eigenstates in the **126** and **10** blocks of the scalar doublet mass matrix (36) were labeled by $m^2_{126\pm}$ and $m^2_{10\pm}$, respectively. In full analogy, let us label the n-loop estimates for these quantities, respectively, by $m^2_{126\pm,(n)}$ and $m^2_{10\pm,(n)}$, where the tree-level case corresponds to $n = 0$. Furthermore, the pure n-loop corrections contributing to these quantities will be denoted by $\delta m^2_{126\pm,(n)}$ and $\delta m^2_{10\pm,(n)}$ for $n \geq 1$, so that

$$m^2_{126\pm,(n+1)} = m^2_{126\pm,(n)} + \delta m^2_{126\pm,(n+1)}, \qquad (55)$$

$$m^2_{10\pm,(n+1)} = m^2_{10\pm,(n)} + \delta m^2_{10\pm,(n+1)}. \qquad (56)$$

As long as loop corrections to the smaller eigenvalues are larger than the required threshold of pretuning in Eq. (40), a milder pretuning condition may be formulated. At any given loop order n, pretuning needs to be performed only down to the (estimated) next-order corrections:

$$|m^2_{126-,(n)}| \lesssim |\delta m^2_{126-,(n+1)}|,$$
$$|m^2_{10-,(n)}| \lesssim |\delta m^2_{10-,(n+1)}|. \qquad (57)$$

This is only a necessary and not a sufficient condition at any given perturbative order, since one relies on the correct alignment of the $(n + 1)$th-order (and higher) corrections. We refer to Eq. (57) as n-PL pretuning, where "n-PL" stands for "nth perturbative level." To this end, We relied on 0-PL pretuning in Sec. III to keep the hope alive beyond tree level. If for any given n (assuming n is low enough that n-loop corrections are larger than the tuning threshold) n-PL pretuning fails, then all-order pretuning is not possible.

A practical limitation of implementing the n-PL pretuning consists in the fact that the left-hand side of Eq. (57) typically corresponds to the highest really computed order, so the corrections of even higher orders on the right-hand side are not readily accessible. The $(n + 1)$th order corrections must thus be estimated in some way.

To keep track of perturbative orders in a mass-square m^2_x, we introduce a loop expansion parameter η_x which should encode the characteristic size of the loop corrections to m^2_x. Needless to say, thus defined η_x depends on the specific parameter-space point as well as on the field x under consideration. The n-loop correction to m^2_x should then obey

$$|\delta m^2_{x,(n)}/m^2_{x,(0)}| \sim \eta^n_x. \qquad (58)$$

Note, however, that this estimate makes sense only when $m^2_{x,(0)}$ is not spuriously small or tuned, i.e., a generic-sized

tree-level mass $m^2_{x,(0)}$ is required. In the case of the lighter doublet in each block, which are to be pretuned, the heavier eigenstate tree-level mass may be (and will be) used as a replacement.

Focusing from now on the shape of the one-loop spectrum (i.e., setting $n = 1$) the 1-PL pretuning must happen down to the level of two-loop corrections whose sizes can be estimated by

$$|\delta m^2_{126-,(2)}| \approx \eta^2_{126}|m^2_{126+,(0)}|,$$
$$|\delta m^2_{10-,(2)}| \approx \eta^2_{10}|m^2_{126+,(0)}|, \qquad (59)$$

where the loop-suppression factors η_{126} and η_{10} in the spirit of Eq. (58) are taken as separate quantities for the blocks M^2_{126} and M^2_{10} (due to different scalar parameters involved in those blocks).

Notice that $m^2_{126+,(0)}$ was used as the tree-level quantity of comparison in both cases, since this is the only eigenvalue that is necessarily of a generic size and, thus, suitable for the task. Namely, the smaller eigenvalues $m^2_{126-,(0)}$ and $m^2_{10-,(0)}$ are pretuned and hence inappropriate, while pretuning in the M^2_{10} block might give a smaller value[9] also for $m^2_{10+,(0)}$.

The loop suppression factors η_{126} and η_{10} relevant for the M^2_{126} and M^2_{10} blocks, respectively, can be estimated by comparing the one-loop corrections to the generic tree-level contribution identified above:

$$\eta_{126} \approx \left| \frac{\delta m^2_{126+,(1)}}{m^2_{126+,(0)}} \right| = \left| \frac{m^2_{126+,(1)} - m^2_{126+,(0)}}{m^2_{126+,(0)}} \right|, \qquad (60)$$

$$\eta_{10} \approx \left| \frac{\delta m^2_{10+,(1)}}{m^2_{126+,(0)}} \right| = \left| \frac{m^2_{10+,(1)} - m^2_{10+,(0)}}{m^2_{126+,(0)}} \right|. \qquad (61)$$

It is also convenient to define suppression ratios R_{126} and R_{10} of the smaller eigenvalues m^2_{126-} and m^2_{10-} at one-loop with respect to the generic tree-level contribution by

$$R_{126} := \left| \frac{m^2_{126-,(1)}}{m^2_{126+,(0)}} \right|, \qquad R_{10} := \left| \frac{m^2_{10-,(1)}}{m^2_{126+,(0)}} \right|, \qquad (62)$$

where the mass $m^2_{126+,(0)}$ was again used as a proxy for the generic (nontuned) tree-level mass square.

Finally, the above insights are combined in the following measures of the quality/strictness of the 1-PL pretuning used in the parameter space scans (smaller Ss indicating better pretuning levels achieved):

---

[9]Unlike $m^2_{126+,(0)}$, a suppressed $m^2_{10+,(0)}$ is possible due to the large number of only loosely restricted new parameters that were introduced through the addition of $\mathbf{10}_C$.

$$S_{126} := \frac{R_{126}}{\eta_{126}^2}, \qquad S_{10} := \frac{R_{10}}{\eta_{10}^2 \times 10^{-2}}. \qquad (63)$$

Note the safety factor 10^{-2} introduced into the denominator of S_{10}; the artificially increased strictness here is meant to compensate for the use of $m_{126+,(0)}^2$ from the **126** sector as the generic tree-level quantity. Since there is no obstruction to attaining doublet pretuning in the M_{10}^2 block (as it is achieved with parameters not directly involved anywhere else in tree-level mass formulas) there is no danger from overly strict tuning demands potentially imposed on S_{10} on other parts of the analysis.

The access to the tree-level and one-loop spectrum allows for explicit numeric evaluation of the η and R quantities, and thus of the measures S_{126} and S_{10}. A successful 1-PL pretuning, i.e., a situation compatible with the basic requirements in Eq. (57), is then characterized by $S_{126}, S_{10} \lesssim 1$, which is a direct consequence of Eqs. (60)–(62). This is also the technical form in which the doublet 1-PL pretuning is imposed as a scan constraint, as reiterated in Sec. IV B.

B. Viability and fine-tuning constraints at one-loop

Before any doublet fine-tuning considerations, we list the general viability constraints that valid parameter points must satisfy. The conditions are analogous to the analysis in [13], which also provides further technical details, while we only give a summary and describe any updates to the conditions below:

(1) Nontachyonicity of the scalar spectrum:

The broken phase of the model has to be developed around a vacuum in which all physical scalar masses are nontachyonic. This criterion is checked on the numerically evaluated one-loop regularized effective masses squared. The computation is updated from the previous study [13] by including the contributions from the $\mathbf{10}_{\mathbb{C}}$, both inside the loops and in the outer legs of diagrams.

(2) Gauge coupling unification:

In GUTs, the SM gauge couplings are required to unify at some high energy scale—the unification scale. To check this, a top-down analysis is performed, where the SO(10) gauge coupling g at the GUT scale is run down to the Z-boson mass scale through a sequence of effective QFTs via renormalization group equations (RGEs). There, we demand the SM gauge couplings to have computed values within $\chi^2 < 9$ of their experimental ones. In contrast to the previous study [13], the unification analysis is upgraded to two-loop RGEs with one-loop threshold corrections, see Appendix B for further technical details.

(3) Perturbativity:

All calculations we perform rely on perturbative methods, so perturbativity criteria have to be devised that every viable point will have to pass. This, in turn, ensures the self-consistency of the computation as a whole.

(a) The global mass-perturbativity test (GMP test) restricts the relative size of one-loop corrections with respect to the average tree-level mass of heavy scalars.[10] As in [13], it is imposed by requiring $\bar{\Delta} < 1$, where the GMP measure $\bar{\Delta}$ is defined by

$$\bar{\Delta} := \frac{\max_{i,j \in \mathrm{HF}}[|M_{ij,\text{one-loop}}^2 - M_{ij,\text{tree}}^2|]}{M_{\text{heavy}}^2}, \qquad (64)$$

where HF is the set of heavy fields.

(b) The next perturbativity requirement demands stability under RG running, since the one-loop effective scalar masses, and consequently the GMP test, possess residual renormalization-scale dependence. Stability of the scalar spectrum is studied via the complete set of one-loop RGEs for dimensionless couplings, see Appendix C. The associated perturbativity measure $\bar{t}$ is defined by

$$\bar{t} := \sqrt{t_+ t_-}, \qquad t_\pm := \log_{10} \frac{\mu_{R\pm}}{\mu_R}, \qquad (65)$$

where μ_R is the initial renormalization scale and $\mu_{R\pm}$ are the upper/lower renormalization scales where a dimensionless scalar coupling hits a Landau-pole instability. We impose $t_+ > 0.5$ on all points, i.e., one can run the points at least half an order of magnitude up in energy without any parameter blowing up. Note that some datasets considered in the following sections have stricter additional requirements implemented on $\bar{t}$.

(c) We compute the one-loop (μ^2, ν^2, τ) position of the vacuum and determine the shift from its initial tree-level position. The test is repeated after running the scalar parameters up half an order of magnitude in scale with the RGEs in Appendix C. As in [13], we require sufficient stability of VEVs, because their shift translates to shifts in one-loop effective scalar masses. Since such a perturbativity test is fast to evaluate, it is used as an initial perturbativity check before the full one-loop spectrum is computed.

---

[10]Heavy scalar fields are those whose masses are not $|\sigma|$−proportional and they do not belong among the would-be Goldstone bosons or pseudo-Goldstone bosons.

(d) The calculation of regularized effective masses (see Appendix A in [13] for details) is not reliable if the PGB masses are overly sensitive to the mass used for these same PGBs inside the loops. We test for this instability by performing an iterative computation of PGB masses, and then by comparing the converged (fixed-point) PGB mass to the initial value. The criterion for iterative convergence of PGBs is technically the same as in [13].

If a point in the parameter space satisfies all the aforementioned viability criteria, it is referred to as viable. While the constraints 1 and 3 are purely theoretical, i.e., required for mathematical consistency or computational stability, constraint 2 is phenomenological in nature. Note also that since there is no unambiguous measure of "perturbativity," the constraints under point 3 are to some degree arbitrary.

In addition to viability constraints, we also impose a limit on the quality of the pretuning in the doublet sector, cf. Sec. II B 2. Specifically, the lightest one-loop eigenvalue in each of the blocks $M^2_{126,\text{one-loop}}$ and $M^2_{10,\text{one-loop}}$ of matrix (36) is required to be at most of the size of two-loop corrections, as was discussed in Sec. IV A. Technically, the relevant 1-PL pretuning conditions are imposed by demanding

$$S_{126} \leq 1, \qquad S_{10} \leq 1, \tag{66}$$

where the S tuning measures were defined in Eq. (63).

Taken all together, a candidate parameter point is considered SM compatible if it is viable (satisfies the general viability criteria of cases 1–3) and its doublets are 1-PL pretuned [satisfying Eq. (66)]. We emphasize that all the aforementioned criteria actually represent necessary and not sufficient conditions: the perturbativity requirements ($\bar{\Delta} < 1$ and $t_+ > 0.5$) are rather mild in the sense that any parameter point under "reasonable" perturbative control should easily fulfil them, and the discarded points are only those that are badly nonperturbative, while the pretuning condition tacitly assumes that two-loop corrections properly align. As we shall see from the results of numeric scans, these necessary conditions already limit the parameter space to very specific regions, which however are in strong tension with stricter perturbativity requirements one might find reasonable to impose (especially in the $\bar{t}$ measure).

C. Input parameters and their ranges

A point in the parameter space of the model under consideration is fully specified by providing the values of the following set of quantities:

$$\{g, \omega_R, |\sigma|, \chi, \lambda_\mathbb{R}, |\lambda_\mathbb{C}|, \arg\lambda_\mathbb{C}, \tau', \xi^2, |\xi'^2|, \arg\xi'^2\}, \tag{67}$$

where g is the unified gauge coupling, ω_R, $|\sigma|$ and χ encode the three relevant symmetry-breaking VEVs via Eqs. (12) and (13), $\lambda_\mathbb{R}$ and $\lambda_\mathbb{C}$ are generic symbols for the 15 real and 14 complex dimensionless couplings in the scalar potential of Eq. (2) and τ', ξ, and ξ' are their dimensionful counterparts related to the extra $\mathbf{10}_\mathbb{C}$, cf. Table II. The other potential parameters μ^2, ν^2, and τ are related to those in the list of Eq. (67) via the stationarity conditions in Eqs. (14)–(16). In total, the list represents a real vector in a 51-dimensional space to be explored.

Besides trivial limits on the values assumed by the periodic parameters $0 \leq \arg(\lambda_\mathbb{C}), \arg(\xi'^2) < 2\pi$, the following perturbativity conditions have been imposed:

$$|\chi|, |\lambda_\mathbb{R}|, |\lambda_\mathbb{C}| < 1,$$
$$1 \text{ GeV} < |\tau'|, |\xi|, |\xi'| < 10\omega_R, \tag{68}$$

along with the correct hierarchy of the physical scales $M_Z < |\sigma| < \omega_R < M_{\text{Pl}}$ (with M_{Pl} and M_Z denoting the Planck and the Z-boson mass, respectively).

D. Results of the numerical analysis

The searches for viable parameter points, as defined in Sec. IV B, with various degrees of pretuning (as measured by S_{126} and S_{10}) were performed using the same methods as in [13], namely the stochastic version of the differential evolution algorithm [55] [version "DE/rand/1" with randomly selected $F \in (0.5, 2)$ for every point]. Every undesired feature or restriction on a parameter point was implemented as a non-negative penalization. The algorithm then iteratively improves upon generations of points by constructing new candidates from the preceding generation. One can use the algorithm in two modes: (i) the minimization mode, in which one tries to find the best possible point with certain features, and (ii) the search mode, where one accepts all newly found points with zero penalization and thus explores the parameter space of points with desired features.

1. A SM-compatible benchmark point

We first present in Table III a SM-compatible benchmark point (BP), i.e., a point that is both viable and satisfies the 1-PL pretuning requirements $S_{10} \leq 1$ and $S_{126} \leq 1$ of Eq. (66). It was obtained as the best point (with the lowest S_{126}) after a considerable computational effort of about 10^5 generations using differential evolution. While the basic viability (as defined in Sec. IV B) and the $S_{10} \leq 1$ criteria were quickly satisfied in the course of minimization, it turned out to be very difficult to satisfy $S_{126} \leq 1$. Ultimately, the minimal attained value corresponds to the BP at

$$S^{\text{BP}}_{126} = 0.915. \tag{69}$$

We remind the reader that S_{126} defines the level of 1-PL pretuning in the M^2_{126} block of the doublet mass matrix in

TABLE III. Parameter input values for the SM-compatible benchmark point. For the values of dimensionful parameters, the "sign-log" function $\lg(x) := \text{sign}(x) \cdot \log_{10}(|x|/\text{GeV})$ has been employed.

Parameter	Value	Parameter	Value
a_0	0.096	$\arg \kappa'_2$	1.917
a_2	0.023	$|\zeta|$	0.483
λ_0	0.139	$\arg \zeta$	0.440
λ_2	0.613	$|\zeta'|$	0.432
λ_4	−0.735	$\arg \zeta'$	1.502
λ'_4	0.040	$|\rho'_0|$	0.076
α	−0.050	$\arg \rho'_0$	1.841
β_4	0.739	$|\psi_0|$	0.238
β'_4	−0.153	$\arg \psi_0$	0.003
$|\gamma_2|$	0.286	$|\psi_1|$	0.177
$\arg \gamma_2$	1.978	$\arg \psi_1$	0.741
$|\eta_2|$	0.355	$|\psi_2|$	0.658
$\arg \eta_2$	0.709	$\arg \psi_2$	1.502
h_2	−0.379	$|\varphi|$	0.016
h'_2	0.301	$\arg \varphi$	0.756
κ_0	0.212	$|\varphi'|$	0.160
κ_2	−0.457	$\arg \varphi'$	1.647
ρ_0	−0.564	g	0.550
ρ_2	−0.707	χ	−0.873
$|h_3|$	0.481	$\lg \omega_R$	14.752
$\arg h_3$	3.472	$\lg \sigma$	11.082
$|h_4|$	0.496	$\lg \tau'$	−15.706
$\arg h_4$	0.104	$\lg |\xi|$	0.189
$|\kappa'_0|$	0.005	$\text{sign}\xi^2$	+1
$\arg \kappa'_0$	1.369	$\lg |\xi'|$	10.853
$|\kappa'_2|$	0.008	$\arg \xi'$	2.409

TABLE IV. The computed datasets of parameter points along with the constraints imposed on top of *viability* in each case. The last column provides the resulting ranges of $\bar{t}$ in the datasets.

Dataset	# of points	Constraints	$\bar{t}$ range
$\mathcal{D}$	20000	Unconstrained	0.36–1.06
$\mathcal{S}^{(2.0)}$	2000	$S_{10} \leq 1,\ S_{126} \leq 2$	0.34–0.49
$\mathcal{S}^{(1.5)}$	2000	$S_{10} \leq 1,\ S_{126} \leq 1.5$	0.34–0.52
$\mathcal{S}^{(1.0)}$	2000	$S_{10} \leq 1,\ S_{126} \leq 1$	0.34–0.41
$\mathcal{T}$	20000	$\bar{t} \geq 1$	1.00–1.20

average), which hardly provides confidence in the perturbative stability of such a point. As it turns out, this is actually a rather general pattern: attainability of the desired level of fine-tuning in the doublet sector strongly correlates with the regions of parameter space that are perturbatively disfavored.

2. Tension between doublet fine-tuning and perturbativity

As the claim above is the central point of the current study, it deserves a closer look and a more detailed analysis. For that sake, we have used the DE algorithm in search mode, i.e., as a tool for exploring the parameter space with different penalization functions corresponding to various thresholds of strictness in the imposed constraints, cf. Table IV.

All points accepted into the datasets are viable as defined in Sec. IV B, but differ in the acceptance threshold either for the level of doublet fine-tuning or for the level of their perturbative stability. To this end, the dataset $\mathcal{D}$ in Table IV is a mere reference sample with no further imposed constraints on S_{10}, S_{126}, and $\bar{t}$, and as such represents a general map of the viable part of parameter space in the $\mathbf{45} \oplus \mathbf{126} \oplus \mathbf{10}_{\mathbb{C}}$ model.[11] The $\mathcal{S}^{(x)}$ datasets for $x = 2.0$, 1.5, and 1.0 conform to the 1-PL pretuning requirement in the M_{10}^2 block of Eq. (36) imposed by $S_{10} \leq 1$, along with an increasingly demanding constraint on the level of 1-PL pretuning in the M_{126}^2 block implemented via the corresponding $S_{126} \leq x$ condition. In essence, such $\mathcal{S}^{(x)}$ datasets explore smaller and smaller neighborhoods around the benchmark point of Table III. Finally, the dataset $\mathcal{T}$ defined by $\bar{t} \geq 1$ explores the parameter-space domains with extended RG-flow perturbativity/stability.

Even a quick glance at Table IV already reveals a tension between the $\mathcal{T}$ dataset and the $\mathcal{S}^{(x)}$ datasets. Indeed, by increasing the demands on the level of pretuning in M_{126}^2 (corresponding to the progression from $x = 2.0$ to $x = 1.0$ in $\mathcal{S}^{(x)}$), the maximum attainable $\bar{t}$ (reflecting the level of

Eq. (36). The 1-PL pretuning difficulty in the **126** sector, however, was not entirely unexpected given the obstructions arising already for 0-PL pretuning in Sec. III. Note that the value in Eq. (69) is not claimed to be the absolute minimum, since the minimization was stopped manually for practical (time) reasons. Nevertheless, given the clear convergence trends in the spread of parameter values in successive generations and the exponentially increasing difficulty in finding better points as the search progressed, any further improvement of the value quoted above—if it exists— should be very small.

In any case, the benchmark point of Table III represents an existence proof that SM-compatible points do in principle exist. However, it is important to recall that the imposed viability criteria of Sec. IV B are not very strict regarding perturbativity; indeed, the corresponding $\bar{t}$ perturbativity measure (65) attains a rather small value at the BP, namely

$$\bar{t}^{\text{BP}} = 0.38. \qquad (70)$$

The RG flow of the scalar parameters thus hits a pole within 0.38 orders of magnitude around the GUT scale (up-down

---

[11]The $\mathcal{D}$ dataset makes it also possible to compare the viable parameter space regions between the current $\mathbf{45} \oplus \mathbf{126} \oplus \mathbf{10}_{\mathbb{C}}$ model and the simpler $\mathbf{45} \oplus \mathbf{126}$ setting studied previously in Ref. [13], see Appendix A.

perturbativity) is diminishing and never reaches above $\bar{t} \sim 0.52$.

The same effect is easily seen in Fig. 1, where each point from the datasets is positioned according to its one-loop "tuning capacity" R_{126} of Eq. (62) and the loop expansion parameter η_{126} of Eq. (60). The color coding for points from different datasets of Table IV in Fig. 1 and later plots is as follows: the points of the unconstrained dataset $\mathcal{D}$ are colored black, the dataset $\mathcal{T}$ with enhanced perturbativity is colored green, while the datasets $\mathcal{S}^{(2.0)}$, $\mathcal{S}^{(1.5)}$, and $\mathcal{S}^{(1.0)}$ with increased tuning attained in the doublet sector are colored blue, magenta, and red, respectively.

Intuitively, the horizontal axis in Fig. 1 indicates how large in relative terms the loop corrections are, while the vertical axis quantifies how much the one-loop mass of the light doublet in the M_{126}^2 block is tuned compared to the corresponding heavy eigenstate. The straight gray line in the figure (corresponding to $R_{126} = \eta_{126}$) represents the points where the one-loop mass of the light doublet is of the size of a typical one-loop contribution, while the orange curve labeled by η^2 defines the upper boundary of the region where the light doublet in M_{126}^2 has been successfully 1-PL *pretuned* down to the typical scale of two-loop effects. One can see that with decreasing x the points of the $\mathcal{S}^{(x)}$ datasets are receding further and further away from the black bulk of the unconstrained dataset $\mathcal{D}$, in accordance with the $S_{126} \leq x$ limits depicted by the relevant $x \cdot \eta^2$ curves, cf. definition in Eq. (63). Notice also that for smaller x the corresponding $\mathcal{S}^{(x)}$ conditions are fulfilled in gradually shrinking domains moving to the right rather than down in the plot, which means that the tuning of the light doublet mass in the M_{126}^2 down to the desired level of typical two-loop effects is achieved by enlarging the expected size of the loop corrections η_{126} rather than suppressing the light eigenstate
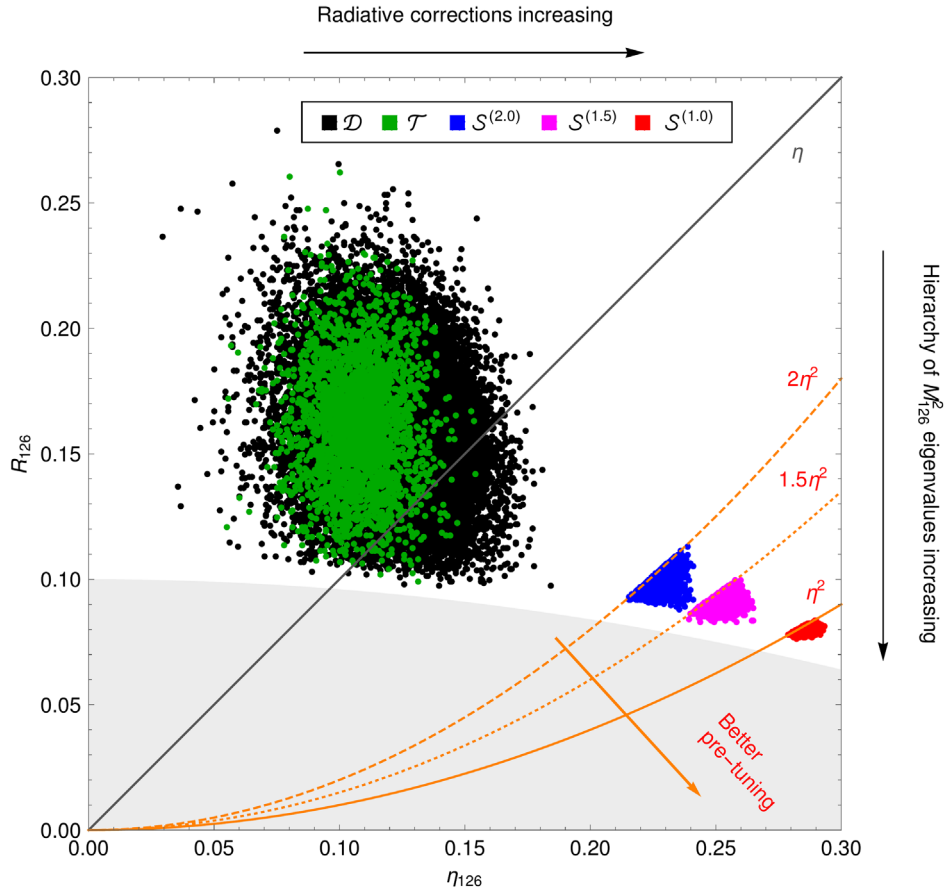

FIG. 1. The plot compares the one-loop tuning ability R_{126} to the loop expansion parameter η_{126} for points in the datasets of Table IV. On the vertical axis the ratio R_{126} determines the relative size of the smaller eigenvalue (i.e., the one to be suppressed as much as possible upon pretuning) of the one-loop M_{126}^2 block of the mass matrix in Eq. (36) as compared to the larger one. Physically, the lower limit on R_{126} at around 0.08 indicates that the two eigenvalues of M_{126}^2 cannot be separated arbitrarily, i.e., points cannot enter the gray region, and hence the only way to attain the desired level of pretuning is to resort to large loop corrections. The estimate of the relative size of such loop corrections (encoded in the η_{126} parameter) for any point in the plot is quantified by its horizontal coordinate. The typical nontuned points are around the gray line $R_{126} = \eta_{126}$, while the properly tuned points satisfying $S_{126} < 1$ are below the orange-colored η^2 curve. The plot makes it clear that the more pretuning in M_{126}^2 is imposed, the more to the right one has to push, and hence larger loop corrections have to be invoked.
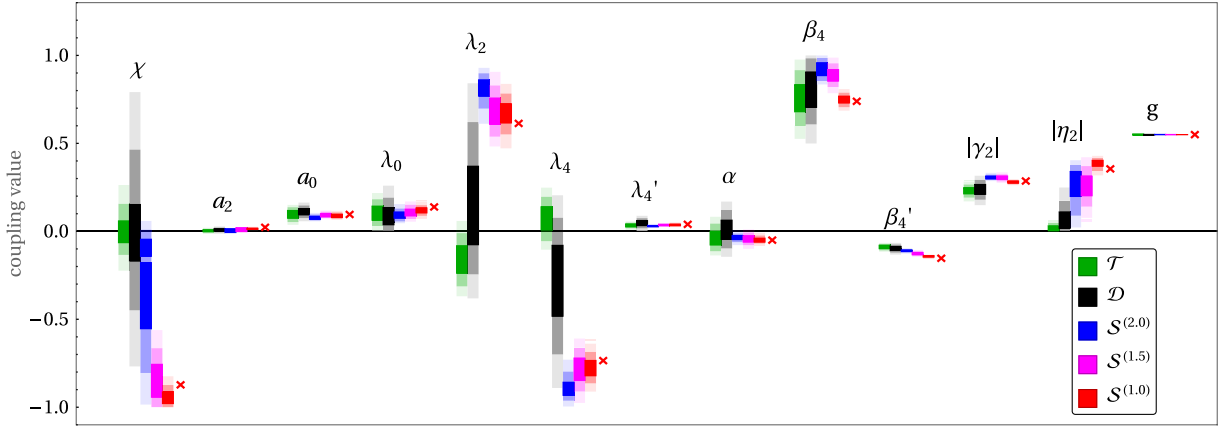
FIG. 2. The ranges of the "old" dimensionless scalar parameters from Table II (i.e., those appearing already in the **45** ⊕ **126** Higgs model of Ref. [13]) along with the universal VEV ratio χ of Eq. (13) for different datasets defined in Table IV. The same general color scheme as in Fig. 1 has been adopted, with decreasing color opacities representing the 1-, 2-, and 3-σ highest density intervals (HDIs) for each quantity. In the Bayesian interpretation these would correspond to HDIs of marginal probability distributions in a single parameter when the sampling of acceptable regions is performed by the differential evolution algorithm. The values corresponding to the benchmark point in Table III are marked by a red cross.

mass. As a consequence, the desired level of fine-tuning in M^2_{126} is attained only for relatively large $\eta_{126} \gtrsim 0.28$, i.e., at the expense of significantly reduced perturbativity (i.e., small $\bar{t}$) of the corresponding points. On the contrary, the points with improved perturbative behavior (corresponding to the $\mathcal{T}$ dataset with $\bar{t} > 1$) generally cluster in the $\eta_{126} < 0.15$ domain, hence indicating a fundamental clash among the two criteria.

The noncompatibility of $\mathcal{S}^{(x)}$ with $\mathcal{T}$ is also apparent from the shape of the parameter space regions that support each of these datasets, see Figs. 2–4. In particular, there is a clear tension between the values of λ_2, λ_4, and $|\eta_2|$, which for the $\mathcal{S}$-type datasets are generally driven towards relatively large (absolute) values, while the same couplings tend to be suppressed across the $\mathcal{T}$ dataset, cf. Fig. 2. This pattern can be understood qualitatively as a consequence of the complexity of the doublet-sector fine-tuning, which generally requires a nontrivial conspiracy among certain parameters; these, in turn, tend to assume values away from their "natural" perturbativity domains in the vicinity of 0.

The tension is further illustrated in the λ_2-λ_4 plane in Fig. 5, which not only depicts the strong anticorrelation of the two parameters across all datasets (a feature that has been observed already in the simplified **45** ⊕ **126** case of Ref. [13]), but makes it very clear that the $\mathcal{T}$ and $\mathcal{S}$ regions are fundamentally incompatible.

Let us conclude this section with a few more comments concerning the results presented above, which may elucidate some further details of the underlying numerical analysis:

(1) Gauge unification constraints along with perturbativity push g, ω_R, and σ into very narrow ranges, cf. Figs. 2 and 4, thus fixing the unification scale and to a large degree also the spectrum of the GUT-scale

gauge leptoquarks. A similar effect is observed for the majority of the "old" dimensionless parameters of the **45** ⊕ **126** Higgs model of Ref. [13], cf. Fig. 2; indeed, these parameters dominate the leading contributions to the masses of most scalar fields in the model, and are hence restricted by viability constraints even in the generic dataset $\mathcal{D}$.

(2) On the other hand, most of the parameters specific to the **10**$_\mathbb{C}$ extension in Fig. 3 stretch over relatively large domains[12]—this should not be surprising, since these parameters influence only a small part of the tree-level spectrum [only the doublet and triplet mass matrices of Eqs. (17) and (18) are affected]. Similarly, the limited number of additional degrees of freedom the extra **10**$_\mathbb{C}$ brings in should not have a big impact on the shape of the RGEs for the "old" scalar parameters, which play a major role in the determination of the perturbative stability domains.

(3) The tension between the viable parameter space domains favored by the dataset $\mathcal{T}$ with enhanced perturbative stability and the fine-tuned datasets $\mathcal{S}^{(x)}$, cf. Figs. 2–4, is not limited to the aforementioned λ_2-λ_4-$|\eta_2|$ subset. Indeed, a similar (though perhaps less pronounced) behavior is observed also in χ, β'_4, κ_2, $|\zeta|$, $|\zeta'|$, and φ'.

(4) There is a relatively large qualitative difference between the behavior of the τ' parameter in the $\mathcal{T}$ and $\mathcal{D}$ datasets as compared to the $\mathcal{S}^{(x)}$ ones, in which the doublet pretuning has been implemented,

---

[12]This behavior, however, is not entirely universal, as some of the new parameters such as φ and φ' still turn out to be quite constrained.
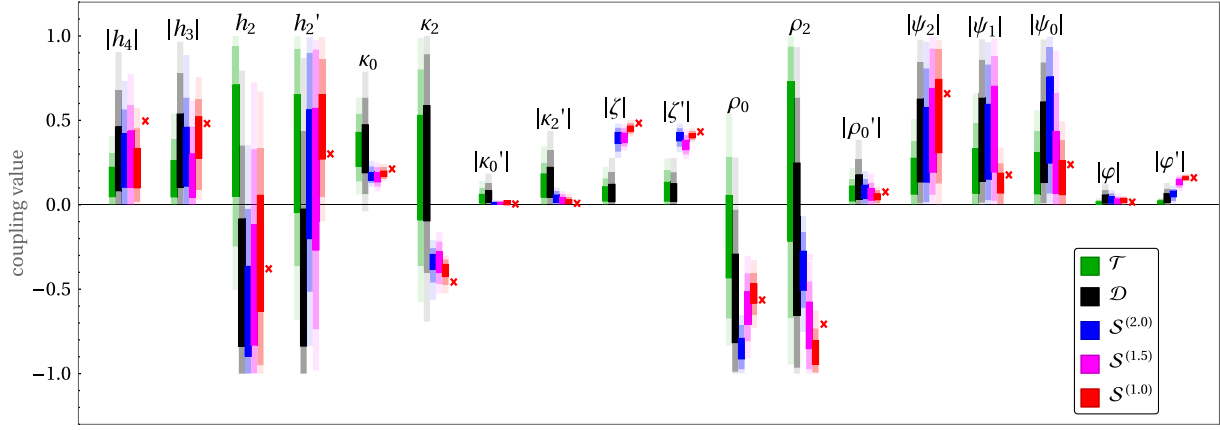
FIG. 3. The HDIs (same conventions as in Fig. 2) for the new dimensionless scalar parameters specific to the model with the added $\mathbf{10}_{\mathbb{C}}$, cf. Table II.
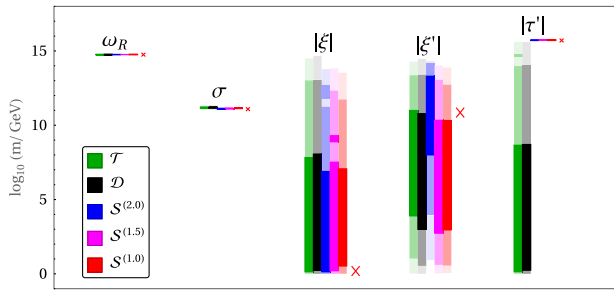

FIG. 4. The HDIs (same conventions as in Fig. 2) for the dimensionful input parameters.
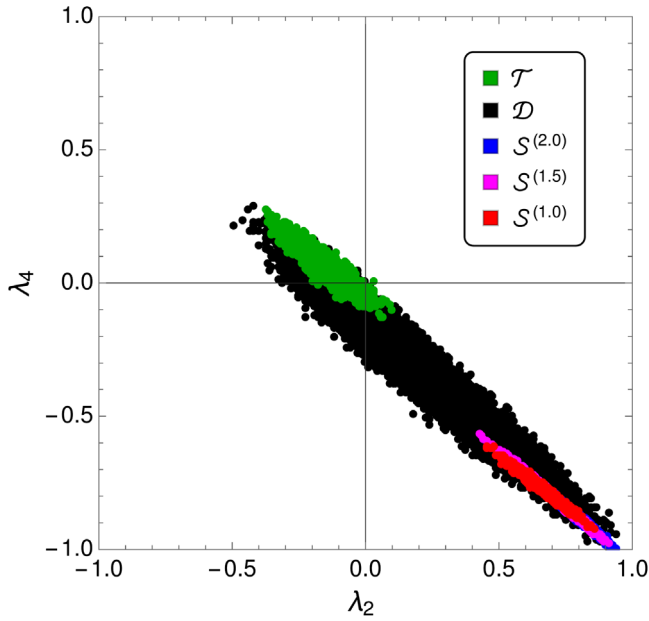

FIG. 5. The correlation plot in the inputs λ_2 and λ_4 for the datasets of Table IV. Enhanced perturbativity (the $\mathcal{T}$ dataset) and 1-PL pretuning (the $\mathcal{S}^{(1.0)}$ dataset) are incompatible.

cf. Fig. 4. This is a mere consequence of the additional algebraic constraint implemented in the M_{10}^2 block of the doublet mass matrix of Eq. (36) in the latter case.

(5) The phases of the complex parameters (such as η_2, γ_2, etc.) are not displayed in Figs. 2 and 3, because the values they assume are not critical to the key observations made above. Nevertheless, as shown in Fig. 6, they are not entirely insensitive to the stringent pretuning constraints imposed in the doublet sector and interesting correlations may emerge, especially for the $\mathcal{S}^{(x)}$ datasets with small x.

V. CONCLUSIONS

The renormalizable SO(10) model with the $\mathbf{45} \oplus \mathbf{126} \oplus \mathbf{10}_{\mathbb{C}}$ Higgs sector (with $\mathbb{C}$ denoting complexification of the relevant representation) has all the features to be considered minimal of its kind, and at the same time potentially realistic. The $\mathbf{45} \oplus \mathbf{126}$ part of its scalar sector is sufficient to implement the desired GUT symmetry breaking down to the SM level, whilst the realistic Yukawa sector fits are known to be possible with $\mathbf{126} \oplus \mathbf{10}_{\mathbb{C}}$ at play.

In practice, however, the model is rather complicated to work with because of the general tachyonic instability of its tree-level scalar spectrum encountered along all physically viable symmetry breaking chains; this in turn makes it purely quantum in nature and calls for a detailed approach with loop corrections taken into account. Moreover, the recent thorough one-loop analysis [13] (focusing on the $\mathbf{45} \oplus \mathbf{126}$ part of the scalar sector) revealed that in major parts of its parameter space the underlying Higgs model suffers from perturbativity issues, which can be alleviated only in a very specific regime featuring an intermediate $\mathrm{SU}(4)_C \times \mathrm{SU}(2)_L \times \mathrm{U}(1)_R$ symmetry stage with the GUT scale localized below 10^{15} GeV.

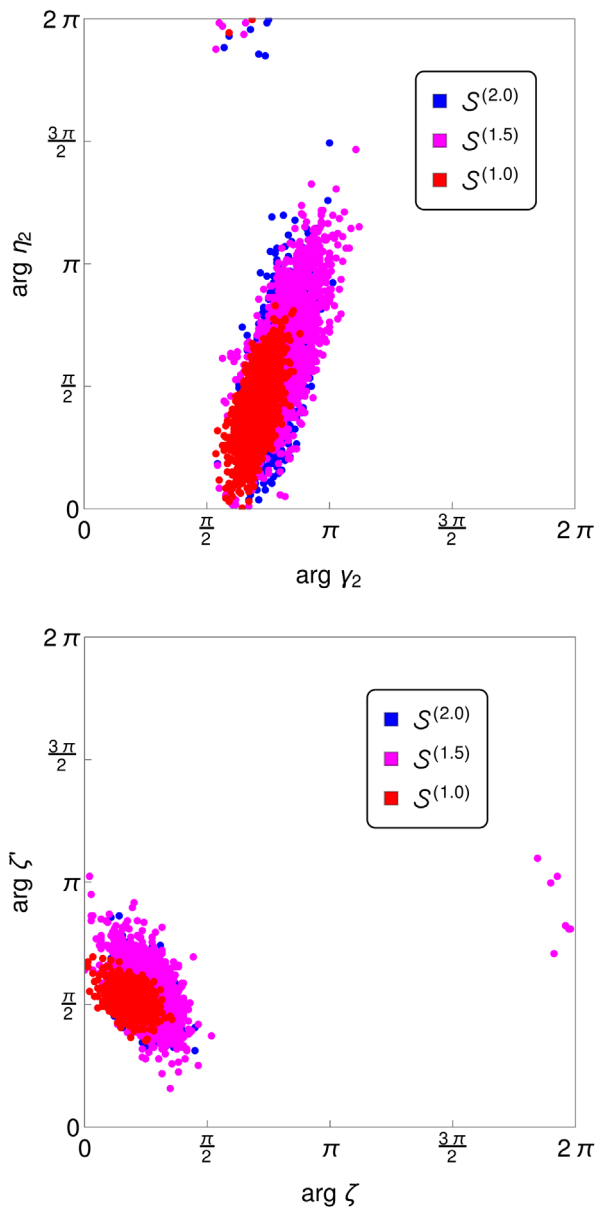Remarkably enough, even with such a low scale governing the $d = 6$ baryon number violating processes,

FIG. 6. Correlations of the phases of two selected pairs of complex parameters (γ_2-η_2 at the top and ζ-ζ' at the bottom) in the $\mathcal{S}^{(x)}$ datasets of Table IV. Note that points from the datasets $\mathcal{D}$ and $\mathcal{T}$ are not shown, since the phases there are uniformly distributed over the entire $[0, 2\pi)$ interval and no interesting correlations emerge.

one should be very careful with discarding the $\mathbf{45} \oplus \mathbf{126}$ type of models on the basis of their alleged incompatibility with existing proton lifetime limits for at least three reasons: in [13] (i) the position of the GUT scale quoted above has been estimated only at the lowest nontrivial order of perturbative expansion; (ii) the possible effects of the additional $\mathbf{10}_{\mathbb{C}}$ present in the minimal potentially realistic setup have not been taken into account; and (iii) little attention has been paid to the special regions in the parameter space which may support accidentally light

thresholds in the GUT desert with a potentially large impact on M_{GUT}, cf. [3,4].

In the current analysis, we carefully addressed points (i) and (ii) above and revealed a remarkable feature of the full $\mathbf{45} \oplus \mathbf{126} \oplus \mathbf{10}_{\mathbb{C}}$ setting that makes the concern (iii) entirely obsolete. In particular, we argued that in the perturbative regime the model cannot accommodate a sufficiently large component of the $\mathbf{126}$ scalar admixed within the SM Higgs doublet; hence, realistic fits of the quark and lepton masses and mixings are inconceivable at the perturbative level in the $\mathbf{45} \oplus \mathbf{126} \oplus \mathbf{10}_{\mathbb{C}}$ scenario. This important observation, hinted at semianalytically already by the doublet mass matrix at tree level (once the one-loop parameter ranges from [13] are taken into account), is fully supported by a detailed numerical analysis of its quantum-level structure.

Beyond the specific GUT model under consideration, this study further illustrates the general importance of quantum corrections in models with a large number of degrees of freedom. Perturbativity considerations of the type implemented in this paper greatly restrict the domain where the model is calculable, and may in fact be incompatible with the set of other demands or limitations imposed on the model (such a fine-tuning).

APPENDIX A: COMPARING THE FULL MODEL WITH THE HIGGS MODEL

In this appendix, we compare the shape of the viable parameter space of the $\mathbf{45} \oplus \mathbf{126}$ Higgs model from [13] with that of the full SO(10) model $\mathbf{45} \oplus \mathbf{126} \oplus \mathbf{10}_{\mathbb{C}}$ studied in this paper.

The full model includes an additional complexified representation $\mathbf{10}_{\mathbb{C}}$ in the scalar sector, and hence new couplings in the scalar potential; for a full list of parameters see Table II. Moreover, unlike in the previous study [13], where the gauge coupling RG analysis has been done at the one-loop level, the unification constraints in the current study have been implemented at two loops.[13] Nevertheless, since $\mathbf{10}_{\mathbb{C}}$ is a small representation that is not involved in

---

[13]Note that in this two-loop unification analysis, the $SU(2)_L$ doublets are assumed to have been successfully fine-tuned, and thus their masses are set to correspond to the physically desired setup: one light eigenstate is identified with the SM Higgs, another lies at around the σ scale, while the remaining two have masses near the GUT scale.

TABLE V.   Comparison of the $\mathcal{B}$ and $\mathcal{D}$ datasets containing viable points within the two variants of the model as discussed in [13] and in the current study.

Dataset	# of points	Scalar content	Gauge RGEs
$\mathcal{B}$ of [13]	30000	**45 $\oplus$ 126**	One-loop
$\mathcal{D}$	20000	**45 $\oplus$ 126 $\oplus$ 10$_{\mathbb{C}}$**	Two-loop

the symmetry breaking, and since the contributions driven by the parameters which are shared by both variants (namely, those of the **45 $\oplus$ 126** sector, cf. Table II) dominate most of the tree-level scalar masses, it has always been implicitly assumed in previous analyses that the corresponding regions of the viable parameter space of the two model variants is very similar, with perhaps only minor quantitative differences. With the results of the current study at hand, this proposition can now be tested.

In practice we compare the dataset $\mathcal{B}$ composed of the viable parameter-space points of the **45 $\oplus$ 126** Higgs model [13] (labeled B_+ therein) with the dataset $\mathcal{D}$ of the viable points of the full **45 $\oplus$ 126 $\oplus$ 10$_{\mathbb{C}}$** model discussed in Sec. IV D 2. At the technical level, these two datasets are compared in Table V.

In analogy to Sec. IV D 2, we display the HDI ranges for the common parameters of the two scenarios of interest (i.e., those parameters denoted as "old" in Table II along with the ratio χ, and the VEVs $|\sigma|$ and ω_R) in Fig. 7. Note that one can view the **45 $\oplus$ 126** Higgs model as a special case of the full **45 $\oplus$ 126 $\oplus$ 10$_{\mathbb{C}}$** setting with all the "new" parameters set to zero.

One can see that the salient features of the new dataset $\mathcal{D}$ are practically identical to those of the old dataset $\mathcal{B}$; hence, their understanding developed in [13] is readily applicable also to the model with **10$_{\mathbb{C}}$** of this study.

There are, however, some minor differences that are worth commenting on:

(1) The VEVs ω_R and σ and coupling g: The quantities ω_R, $|\sigma|$, and g are essentially determined by the gauge coupling unification pattern, so small shifts in these parameters between the $\mathcal{B}$ and $\mathcal{D}$ dataset are expected due to the upgrade from one- to two-loop RGEs. According to [29], the GUT scale (and thus ω_R) is expected to decrease for the two-loop case, which is indeed seen in Fig. 7. Interestingly, the slight increase in $|\sigma|$ asserted in [29] is not reproduced here; rather a slight tendency for its decrease is observed. This can be tracked down to the threshold effects associated to the pretuned doublet at the intermediate scale of the $\mathcal{D}$ dataset, which counteract the generic behavior predicted by [29].

(2) The "old" parameters: Interestingly, the spread in all the "old" dimensionless parameters of Table II as well as in the ratio χ and the VEV $|\sigma|$ tend to shrink in the $\mathcal{D}$ dataset (as compared to $\mathcal{B}$ of [13]), cf. Fig. 7. This may sound a bit counterintuitive, since the new couplings, due to the extra **10$_{\mathbb{C}}$** in the full model, might be expected to help with countering large perturbative corrections, thus presumably extending these ranges. It turns out though that two-loop gauge unification in combination with tachyonicity and perturbativity constraints actually leads to more stringent restrictions. The central values of the "old" parameters remain largely unchanged, small shifts are seen only in a_2, β'_4, and γ_2.

(3) Phases of complex parameters: The distributions of the phases arg η_2 and arg γ_2 across both the $\mathcal{B}$ and $\mathcal{D}$ datasets, cf. Tables IV and V, are almost uniform over the entire $[0, 2\pi)$ domain and, hence, they have been omitted from the plots.
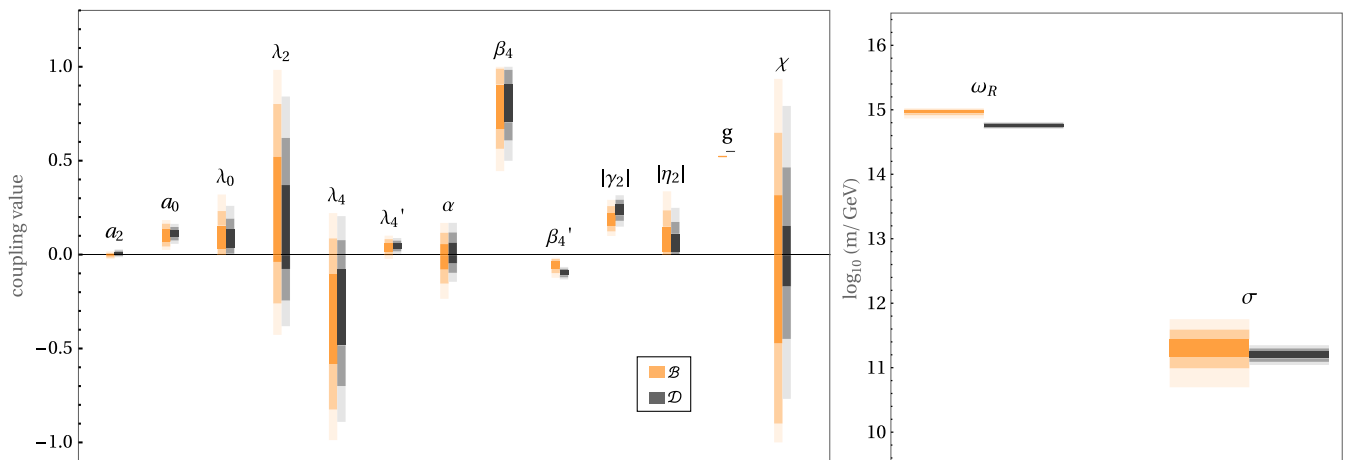

FIG. 7.   The 1-, 2-, and 3-σ HDI ranges (distinguished by decreasing opacity) of the old dimensionless scalar parameters with ratio χ (left panel) and VEVs ω_R, σ (right panel) for datasets $\mathcal{B}$ and $\mathcal{D}$.

APPENDIX B: TWO-LOOP GAUGE UNIFICATION CONSTRAINTS

The requirement of unification of gauge couplings at $M_{\rm GUT}$ is implemented for any given point in the parameter space via the standard goodness-of-fit χ^2 measure applied to the values of the three SM running gauge couplings evolved from the common GUT-scale value g down to the electroweak scale. This evolution is governed by the relevant two-loop RG flow passing through several thresholds corresponding to a sequence of effective theories, which in the $\omega_{BL} \to 0$ limit (and for $|\sigma| \ll |\omega_R|$) can be written as

$$\mathcal{T}_{10} \xrightarrow{M_{\rm GUT}} \mathcal{T}_{421+} \xrightarrow{M_{\rm PGB}} \mathcal{T}_{421} \xrightarrow{M_\sigma} \mathcal{T}_{321}, \qquad \text{(B1)}$$

where $M_{\rm GUT} > M_{\rm PGB} > M_\sigma$ denote the three crucial matching scales around which various heavy fields are integrated out, cf. Table VI. Note that the gauge structure changes only at $M_{\rm GUT}$ and M_σ, where the heavy gauge fields effectively disappear, but there is no such change at $M_{\rm PGB}$, where only the scalar PGBs drop from the spectrum. The details of the entire procedure are summarized below in three subsections: the structure of the four effective theories of Eq. (B1) and the RGEs for the corresponding gauge couplings are given in Appendix B 1, the matching conditions in Appendix B 2, and the details of their practical implementation in Appendix B 3.

1. Two-loop RGEs for gauge couplings

In an effective field theory with the gauge symmetry composed of N factors $G_1 \times G_2 \times \ldots \times G_N$ [with at most one $U(1)$ involved], while the fermions and scalars are in irreducible representations F_f and S_s, the two-loop evolution equations for the gauge couplings g_i ($i = 1 \ldots N$) can be written as [29,56]

$$\frac{d}{dt}\alpha_i^{-1} = -\frac{1}{2\pi}\left(a_i + \frac{1}{4\pi}\sum_{j=1}^{N} b_{ij}\alpha_j - \frac{1}{16\pi^2}\sum_f \eta_{F_f} Y_4^{(i)}(F_f)\right), \tag{B2}$$

where $\alpha_i = g_i^2/4\pi$ and

$$t = \log\left(\frac{\mu_R}{M_Z}\right), \tag{B3}$$

with μ_R denoting the renormalization scale. The one- and two-loop coefficients a_i and b_{ij} are defined as

$$a_i = -\frac{11}{3}C_i(G_i) + \frac{1}{3}\sum_s \eta_{S_s} D_i(S_s) + \frac{2}{3}\sum_f \eta_{F_b} D_i(F_f), \tag{B4}$$

$$b_{ij} = 4\sum_s \eta_{S_s} D_i(S_s)C_j(S_s) + 2\sum_f \eta_{F_f} D_i(F_f)C_j(F_f)$$
$$+ \delta_{ij}\left[-\frac{34}{3}C_i(G_i)^2 + \frac{2}{3}\sum_s \eta_{S_s} D_i(S_s)C_i(G_i) + \frac{10}{3}\sum_f \eta_{F_f} D_i(F_f)C_i(G_i)\right]. \tag{B5}$$

In the sums above, the indices f and s run over all fermionic and scalar representations involved, D_i and C_i label the Dynkin index and quadratic Casimir with respect to the gauge factor G_i of the representation in their arguments, $\eta_S = \frac{1}{2}$ or 1 for real or complex scalars and

TABLE VI. The sequence of different effective-theory stages defining the two-loop RG evolution of gauge couplings from the GUT scale down to the EW scale. For each stage the labels of the corresponding gauge couplings are listed along with the relevant fermionic and scalar degrees of freedom [cf. Eqs. (B6)–(B10)], as well as the one- and two-loop beta coefficients a_i and b_{ij}.

Theory	Symmetry	Couplings	Fermions	Scalars	a_i	b_{ij}
$\mathcal{T}_{10}$	SO(10)	(α_{10})	$3 \times \mathbf{16}_F$	$\mathbf{45}_\mathbb{R} \oplus \mathbf{126}_\mathbb{C} \oplus \mathbf{10}_\mathbb{C}$	(-12)	$\left(\frac{3223}{2}\right)$
$\mathcal{T}_{421+}$	$SU(4)_C \times SU(2)_L \times U(1)_R$	$(\alpha_C, \alpha_L, \alpha_R)$	$3 \times \mathbf{F}_{421}$	$\mathbf{S}_{421} \oplus \mathbf{S}_{421+}$	$\left(-\frac{19}{3}, -\frac{1}{3}, 10\right)$	$\begin{pmatrix} \frac{1019}{6} & \frac{57}{2} & \frac{43}{2} \\ \frac{285}{2} & \frac{143}{3} & 8 \\ \frac{645}{2} & 24 & 51 \end{pmatrix}$
$\mathcal{T}_{421}$	$SU(4)_C \times SU(2)_L \times U(1)_R$	$(\alpha_C, \alpha_L, \alpha_R)$	$3 \times \mathbf{F}_{421}$	$\mathbf{S}_{421}$	$\left(-7, -\frac{2}{3}, 10\right)$	$\begin{pmatrix} \frac{265}{2} & \frac{57}{2} & \frac{43}{2} \\ \frac{285}{2} & \frac{115}{3} & 8 \\ \frac{645}{2} & 24 & 51 \end{pmatrix}$
$\mathcal{T}_{321}$	$SU(3)_c \times SU(2)_L \times U(1)_Y$	$(\alpha_c, \alpha_L, \alpha_1)$	$3 \times \mathbf{F}_{321}$	$\mathbf{S}_{321}$	$\left(-7, -\frac{19}{6}, \frac{41}{10}\right)$	$\begin{pmatrix} -26 & \frac{9}{2} & \frac{11}{10} \\ 12 & \frac{35}{6} & \frac{9}{10} \\ \frac{44}{5} & \frac{27}{10} & \frac{199}{50} \end{pmatrix}$

$\eta_F = \frac{1}{2}$ or 1 for Weyl or Dirac fermions, respectively. The specific values of a_i and b_{ij} for different effective theories in the chain of Eq. (B1) are given in Table VI, with a few accompanying definitions (B6)–(B10) provided below:

$$\mathbf{F}_{421} \equiv (4, 2, 0) \oplus \left(\bar{4}, 1, +\frac{1}{2}\right) \oplus \left(\bar{4}, 1, -\frac{1}{2}\right), \qquad \text{(B6)}$$

$$\mathbf{F}_{321} \equiv \left(3, 2, \frac{1}{6}\right) \oplus \left(\bar{3}, 1, -\frac{2}{3}\right) \oplus \left(\bar{3}, 1, +\frac{1}{3}\right) \oplus$$
$$\oplus \left(1, 2, -\frac{1}{2}\right) \oplus (1, 1, +1), \qquad \text{(B7)}$$

$$\mathbf{S}_{421} \equiv (\overline{10}, 1, -1)_{\mathbb{C}} \oplus \left(15, 2, +\frac{1}{2}\right)_{\mathbb{C}} \oplus \left(1, 2, +\frac{1}{2}\right)_{\mathbb{C}}, \quad \text{(B8)}$$

$$\mathbf{S}_{421+} \equiv (1, 3, 0)_{\mathbb{R}} \oplus (15, 1, 0)_{\mathbb{R}}, \qquad \text{(B9)}$$

$$\mathbf{S}_{321} \equiv \left(1, 2, +\frac{1}{2}\right)_{\mathbb{C}}. \qquad \text{(B10)}$$

The Yukawa contribution $Y_4^{(i)}(F_f)$ in Eq. (B2) is computed via [29]

$$Y_4^{(i)}(F_f) = \sum_y \text{Tr}[C_i(F_f)\mathbf{Y}_y\mathbf{Y}_y^\dagger]/\dim(G_i), \qquad \text{(B11)}$$

where the sum runs over all Yukawa matrices in the theory (indexed by y), and the trace has to be taken over all gauge and family indices. To avoid unnecessary complication with Yukawa matching, and assuming the full dominance of the top Yukawa coupling y_t, the last term in Eq. (B2) is approximated by

$$\sum_f \eta_{F_f} Y_4^{(i)}(F_f) = \tilde{b}_i y_t^2, \qquad \text{(B12)}$$

with $\tilde{b}_i = \{2, \frac{3}{2}, \frac{17}{10}\}$ for the $\mathcal{T}_{321}$ stage and $\tilde{b}_i = \{2, 2, 2\}$ for the $\mathcal{T}_{421}$ and $\mathcal{T}_{421+}$ stages. For the same reason the running of the y_t parameter is approximated by a purely SM-like evolution

$$\frac{d}{dt} y_t = \frac{1}{16\pi^2} \frac{9}{2} y_t^3 - \frac{1}{4\pi} y_t \sum_{i \in \{c, L, 1\}} \tilde{a}_i \alpha_i, \qquad \text{(B13)}$$

where $\{\alpha_c, \alpha_L, \alpha_1\}$ are the three SM gauge coupling factors (calculated in the $\mathcal{T}_{421}$ and $\mathcal{T}_{421+}$ stages from the values of $\{\alpha_C, \alpha_L, \alpha_R\}$ as $\alpha_1^{-1} = \frac{3}{5}\alpha_R^{-1} + \frac{2}{5}\alpha_C^{-1}$ and $\alpha_c^{-1} = \alpha_C^{-1}$) and $\{\tilde{a}_c, \tilde{a}_L, \tilde{a}_1\} = \{8, \frac{9}{4}, \frac{17}{20}\}$. Several additional remarks are noteworthy here:

(1) Since the procedure of top-down unification starts at M_{GUT}, the a and b factors for the unified theory $\mathcal{T}_{10}$

are not needed. We provide them regardless for completeness.

(2) The representations listed in Eqs. (B6)–(B10) are written in notation appropriate for the symmetry at that stage. The index $\mathbb{R}$ or $\mathbb{C}$ for a scalar representation denotes whether it carries real or complex degrees of freedom, respectively.

(3) The presence of the scalar set $\mathbf{S}_{421}$ [cf. Eq. (B8)] in the $\mathcal{T}_{421}$ and $\mathcal{T}_{421+}$ stages is consistent with the extended survival hypothesis. Indeed, the breakdown of $\text{SU}(4)_C$ proceeds through the first [$\text{SU}(2)_L$-singlet] representation therein, whilst the latter two multiplets [$\text{SU}(2)_L$ doublets] accommodate the SM Higgs doublet, cf. Sec. II B. The extra $\mathbf{S}_{421+}$ scalars present at the $\mathcal{T}_{421+}$ stage are the PGBs.

(4) $\mathcal{T}_{321}$ is the usual Standard Model that includes one Higgs doublet. Note that the hypercharges in Eqs. (B7) and (B10) refer to the values of Y in the usual SM normalization (with $Q = T_L^3 + Y$), while the traditional GUT normalization with $\alpha_1 = \frac{5}{3}\alpha_Y$ is used for the a and b coefficients in Table VI.

(5) The approximate treatment of Yukawa contributions via Eqs. (B12) and (B13) is justified by noting their minuscule effect on unification. In particular, in a top-down fit of the low energy gauge coupling data, switching on separately the gauge and Yukawa part of the two-loop RGE induces a relative change of 1.5% and 10^{-4}, respectively, in the log of the GUT scale [in the quantity $\log_{10}(M_{\text{GUT}}/\text{GeV})$] compared to the fit with one-loop RGE. The Yukawa contribution in Eq. (B2) is thus a negligible part of the two-loop RGE upgrade, and hence the details of its treatment have little impact on the current analysis.

2. Matching conditions for gauge couplings

At each of the symmetry-breaking steps defined in Table VI, the gauge couplings associated to the higher-scale gauge symmetry $G = G_1 \times G_2 \times \ldots \times G_N$ (encoded in $\alpha_j \equiv g_j^2/4\pi$ with $j = 1\ldots N$) must be matched to those of the lower-scale effective theory with the gauge structure $\tilde{G} = \tilde{G}_1 \times \tilde{G}_2 \times \ldots \times \tilde{G}_M$ (and couplings $\tilde{\alpha}_i$, $i = 1\ldots M$). The corresponding matching conditions then read[14] [56–58]

$$\tilde{\alpha}_i^{-1}(\mu_R) = \sum_{j=1}^N c_{ij}\alpha_j^{-1}(\mu_R) - 4\pi\lambda_i(\mu_R), \qquad \text{(B14)}$$

where μ_R is the matching scale, the $c_{ij} \in \mathbb{R}$ coefficients are determined by the embedding of $\tilde{G}$ into G (see Table VII), and the one-loop threshold factors λ_i are defined as

---

[14]Here it is implicitly assumed that there is at most one Abelian factor among the G_js, and at most one among $\tilde{G}_i$s. This ensures that there is no kinetic mixing between different U(1), which simplifies the situation significantly.

TABLE VII.   The inputs of the matching conditions in Eqs. (B14) and (B15) when transitioning from the theory $\mathcal{T}$ to $\tilde{\mathcal{T}}$ at the matching scale μ_R. The c_{ij} coefficients entering Eq. (B14) and the fields to be integrated out at μ_R [i.e., those that contribute to the threshold corrections in Eq. (B15)] are given for each transition in the effective-theory chain of Eq. (B1). The index $\mathbb{C}/\mathbb{R}$ reflects the complex/real nature of the scalars in the relevant representation, while $G_{\mathbb{C}}/G_{\mathbb{R}}$ and $WGB_{\mathbb{C}}/WGB_{\mathbb{R}}$ indicate complexity/reality of gauge bosons and the corresponding scalar WGBs, respectively.

μ_R	$\mathcal{T} \to \tilde{\mathcal{T}}$	c_{ij}	Fields to integrate out
M_{GUT}	$\mathcal{T}_{10} \to \mathcal{T}_{421+}$	$\begin{pmatrix} 1 \\ 1 \\ 1 \end{pmatrix}$	$(6,2,+\frac{1}{2})_{G_{\mathbb{C}}} \oplus (1,1,+1)_{G_{\mathbb{C}}} \oplus (6,2,+\frac{1}{2})_{WGB_{\mathbb{C}}} \oplus (1,1,+1)_{WGB_{\mathbb{C}}},$ $(\overline{10},1,+1)_{\mathbb{C}} \oplus (\overline{10},1,0)_{\mathbb{C}} \oplus (10,3,0)_{\mathbb{C}} \oplus (15,2,-\frac{1}{2})_{\mathbb{C}} \oplus (6,1,0)_{\mathbb{C}} \oplus (6,1,0)_{\mathbb{C}} \oplus (1,2,+\frac{1}{2})_{\mathbb{C}}$
M_{PGB}	$\mathcal{T}_{421+} \to \mathcal{T}_{421}$	$\begin{pmatrix} 1 & 0 & 0 \\ 0 & 1 & 0 \\ 0 & 0 & 1 \end{pmatrix}$	$(1,3,0)_{\mathbb{R}} \oplus (15,1,0)_{\mathbb{R}}$
M_{σ}	$\mathcal{T}_{421} \to \mathcal{T}_{321}$	$\begin{pmatrix} 1 & 0 & 0 \\ 0 & 1 & 0 \\ \frac{2}{5} & 0 & \frac{3}{5} \end{pmatrix}$	$(3,1,+\frac{2}{3})_{G_{\mathbb{C}}} \oplus (1,1,0)_{G_{\mathbb{R}}} \oplus (3,1,+\frac{2}{3})_{WGB_{\mathbb{C}}} \oplus (1,1,0)_{WGB_{\mathbb{R}}}, (\bar{6},1,-\frac{1}{3})_{\mathbb{C}} \oplus (1,1,0)_{\mathbb{R}} \oplus (8,2,+\frac{1}{2})_{\mathbb{C}} \oplus (\bar{3},2,-\frac{1}{6})_{\mathbb{C}} \oplus (3,2,+\frac{7}{6})_{\mathbb{C}} \oplus (1,2,\frac{1}{2})_{\mathbb{C}}$

$$\lambda_i(\mu_R) = \frac{1}{8\pi^2}\left[\sum_g \tilde{D}_i(V_g)\left(\frac{1}{6} - \frac{11}{3}\log\frac{M_{V_g}}{\mu_R}\right)\right.$$
$$+ \frac{4}{3}\sum_f \eta_{F_f}\tilde{D}_i(F_f)\log\frac{M_{F_f}}{\mu_R}$$
$$\left.+ \frac{1}{3}\sum_s \eta_{S_s}\tilde{D}_i(S_s)\log\frac{M_{S_s}}{\mu_R}\right]. \tag{B15}$$

Here the sums over g, f, and s, respectively, run over all irreducible representations (of the $\tilde{G}$ symmetry) containing massive gauge bosons V_g, fermions F_f, and scalars S_s that are integrated out at μ_R. The η_{F_f} and η_{S_s} coefficients are defined as in Eqs. (B4) and (B5) and $\tilde{D}_i$ are Dynkin indices relative to the $\tilde{G}_i$ factor in $\tilde{G}$. The M_{V_g}, M_{F_f}, and M_{S_s} quantities in arguments of logs denote the (tree-level) masses of the corresponding fields; the would-be Goldstone bosons are formally included with a mass equal to the mass of the associated gauge fields. More specific information on the elements entering the formulas above at different matching scales is given in Table VII.

Note that the threshold corrections λ_i effectively take into account the details of the spectrum of the fields integrated out around the matching scale μ_R, which is in principle arbitrary (as long as it is not far from the typical mass scale of the fields being integrated out), since its specific position influences the result only at next order in the perturbative expansion. The details of determination of the matching scales M_{GUT}, M_{PGB}, and M_{σ} are given in Sec. B 3.

3. Implementation of the two-loop gauge unification constraints

For the sake of explicitness, a short note on the practical implementation of two-loop gauge unification constraints is provided in the form of a step-by-step procedure, which is applied to every parameter-space point from the numerical scans described in Sec. IV:

(1) The unification-scale value of the unified gauge coupling is called g and it is one of the inputs. Then M_{GUT} is calculated as the barycenter of the ω_R-proportional dominant terms of the tree-level gauge boson masses:

$$M_{\text{GUT}} = \sqrt{\frac{8}{13}}g\omega_R. \tag{B16}$$

The GUT-scale initial condition for the top quark Yukawa coupling is always taken to be $y_t(M_{\text{GUT}}) = 0.494$, which is the value obtained from the bottom-up y_t running in the SM (at one loop) to 10^{15} GeV.

(2) Match $\mathcal{T}_{10} \to \mathcal{T}_{421+}$ at M_{GUT}, including threshold corrections.

(3) Run $(\alpha_C, \alpha_L, \alpha_R)$ and y_t in the $\mathcal{T}_{421+}$ framework from M_{GUT} to the pseudo-Goldstone-boson scale M_{PGB}, which is defined as the weighted average of the PGB masses:

$$M_{\text{PGB}} = \frac{\sum_X d_X M_X}{\sum_X d_X}, \tag{B17}$$

where the sum goes over all PGB multiplets X (cf. row 2 of Table VII), while d_X and M_X denote the size (in terms of real degrees of freedom) and mass of X, respectively.

(4) Match $\mathcal{T}_{421+} \to \mathcal{T}_{421}$ at M_{PGB}, including threshold corrections.

(5) Run $(\alpha_C, \alpha_L, \alpha_R)$ and y_t in the theory $\mathcal{T}_{421}$ from M_{PGB} to the seesaw scale M_{σ}. The scale M_{σ} is determined as the barycenter of σ-proportional tree-level gauge boson masses, i.e.,

$$M_{\sigma} = \sqrt{\frac{22}{7}}g|\sigma|. \tag{B18}$$

(6) Match $\mathcal{T}_{421} \to \mathcal{T}_{321}$ at M_σ, including threshold corrections.

(7) Run $(\alpha_c, \alpha_L, \alpha_1)$ and y_t in the theory $\mathcal{T}_{321}$ from M_σ to the Z-boson mass $M_Z = 91.19$ GeV [59].

(8) Calculate χ^2 based on the computed gauge couplings $\alpha_c(M_Z), \alpha_L(M_Z), \alpha_1(M_Z)$ compared to their experimental values [60–64]

$$\alpha_c^{-1}(M_Z) = 8.550 \pm 0.065, \tag{B19}$$

$$\alpha_L^{-1}(M_Z) = 29.6261 \pm 0.0051, \tag{B20}$$

$$\alpha_1^{-1}(M_Z) = 59.1054 \pm 0.0031. \tag{B21}$$

A value of $\chi^2 \leq 9$ is required for the parameter space point to pass the unification test without penalization.

Note that the procedure above assumes a spectrum where doublet fine-tuning has been hypothetically achieved along the lines of Sec. IV A. In that case, out of the four SM-doublet scalars $(1, 2, +\frac{1}{2})$ in the model, two have masses around the unification scale M_{GUT}, one has a mass around the seesaw scale M_σ, and the remaining mass is at the level of the SM Higgs. For that sake, we fix the corresponding masses by hand to

$$M_S\left(1, 2, +\frac{1}{2}\right)_4 = M_S\left(1, 2, +\frac{1}{2}\right)_3 = M_{\mathrm{GUT}}, \tag{B22}$$

$$M_S\left(1, 2, +\frac{1}{2}\right)_2 = M_\sigma 10^{z/2}, \tag{B23}$$

$$M_S\left(1, 2, +\frac{1}{2}\right)_1 = 125 \text{ GeV}, \tag{B24}$$

where the newly introduced parameter z [assuming random values in the $(-1, 1)$ interval] models the possible offsets of the mass of the $(1, 2, +\frac{1}{2})_2$ scalar around the M_σ scale. The specific choice of z does not influence the results of the current study in any appreciable way.

APPENDIX C: β FUNCTIONS OF SCALAR COUPLINGS OF THE $45 \oplus 126 \oplus 10_{\mathbb{C}}$ MODEL

The list of one-loop β functions of all dimensionless couplings governing the scalar potential of the $45 \oplus 126 \oplus 10_{\mathbb{C}}$ model (i.e., the $D = 0$ couplings of Table II) is given below. The computation was performed using the effective potential method described in Appendix C of Ref. [13].

The β functions for the real couplings of the "old" setting of Table II [i.e., those entering the V_{45}, V_{126}, and V_{mix} terms of Eq. (2)], extended for the presence of $10_{\mathbb{C}}$, read

$$16\pi^2 \beta_{a_0} = 126\alpha^2 + 56\alpha\beta_4 + 112\alpha\beta_4' + 424a_0^2 + 152a_0a_2 + 12a_2^2 + \frac{33}{2}\beta_4^2 + 26\beta_4\beta_4' + 106\beta_4'^2$$
$$- 56|\gamma_2|^2 + 12|\zeta|^2 + 12|\zeta'|^2 + 10\kappa_0^2 + 4\kappa_0\kappa_2 + 40|\kappa_0'|^2 + 8\kappa_0'\kappa_2'^* + 8\kappa_0'^*\kappa_2' + \frac{9}{2}g^4 - 96a_0g^2, \tag{C1}$$

$$16\pi^2 \beta_{a_2} = 96a_0a_2 + 76a_2^2 - 5\beta_4^2 + 60\beta_4\beta_4' - 100\beta_4'^2 + 560|\gamma_2|^2 - 24|\zeta|^2 - 24|\zeta'|^2 + 4\kappa_2^2 + 16|\kappa_2'|^2 + 3g^4 - 96a_2g^2, \tag{C2}$$

$$16\pi^2 \beta_{\lambda_0} = 90\alpha^2 + 40\alpha\beta_4 + 80\alpha\beta_4' + 10\beta_4^2 + 80\beta_4'^2 + 520\lambda_0^2 + 2440\lambda_0\lambda_2 + 2680\lambda_0\lambda_4 + 4960\lambda_0\lambda_4'$$
$$+ 3460\lambda_2^2 + 7880\lambda_2\lambda_4 + 12320\lambda_2\lambda_4' + 4660\lambda_4^2 + 13280\lambda_4\lambda_4' + 16960\lambda_4'^2 + 10\rho_0^2 + 10\rho_0\rho_2$$
$$+ 40|\rho_0'|^2 + 5\rho_2^2 + 3840|\varphi|^2 + 3840|\varphi'|^2 + \frac{135}{2}g^4 - 150\lambda_0g^2, \tag{C3}$$

$$16\pi^2 \beta_{\lambda_2} = -4\beta_4^2 - 32\beta_4'^2 - 32|\gamma_2|^2 - 1264|\eta_2|^2 + 24\lambda_0\lambda_2 - 180\lambda_2^2 - 584\lambda_2\lambda_4 - 160\lambda_2\lambda_4' - 656\lambda_4^2$$
$$- 800\lambda_4\lambda_4' - 2560\lambda_4'^2 - \rho_2^2 - 4|\psi_0|^2 - 2|\psi_1|^2 - 4|\psi_2|^2 - 1408|\varphi|^2 - 1408|\varphi'|^2 - 24g^4 - 150\lambda_2g^2, \tag{C4}$$

$$16\pi^2 \beta_{\lambda_4} = 2\beta_4^2 + 16\beta_4'^2 + 32|\gamma_2|^2 + 1328|\eta_2|^2 + 24\lambda_0\lambda_4 + 16\lambda_2^2 + 112\lambda_2\lambda_4 + 128\lambda_2\lambda_4' + 268\lambda_4^2$$
$$+ 640\lambda_4\lambda_4' + 1408\lambda_4'^2 + 4|\psi_0|^2 + 2|\psi_1|^2 + 4|\psi_2|^2 + 768|\varphi|^2 + 768|\varphi'|^2 + 12g^4 - 150\lambda_4g^2, \tag{C5}$$

$$16\pi^2 \beta_{\lambda_4'} = 4\beta_4\beta_4' - 4\beta_4'^2 + 32|\eta_2|^2 + 24\lambda_0\lambda_4' - 4\lambda_2^2 - 8\lambda_2\lambda_4 - 16\lambda_2\lambda_4' + 4\lambda_4^2 + 112\lambda_4\lambda_4' - 240\lambda_4'^2$$
$$- 416|\varphi|^2 - 416|\varphi'|^2 - 3g^4 - 150\lambda_4'g^2, \tag{C6}$$

$$
\begin{aligned}
16\pi^2\beta_\alpha ={}& 8\alpha^2 + 508\alpha\lambda_0 + 1220\alpha\lambda_2 + 1340\alpha\lambda_4 + 2480\alpha\lambda_4' + 376\alpha a_0 + 80a_0\beta_4 + 160a_0\beta_4' + 76\alpha a_2 \\
&+ 16a_2\beta_4 + 32a_2\beta_4' + 4\beta_4^2 + 16\beta_4\beta_4' + 112\beta_4\lambda_0 + 272\beta_4\lambda_2 + 288\beta_4\lambda_4 + 512\beta_4\lambda_4' + 144\beta_4'^2 \\
&+ 224\beta_4'\lambda_0 + 544\beta_4'\lambda_2 + 576\beta_4'\lambda_4 + 1024\beta_4'\lambda_4' + 64|\gamma_2|^2 + 20\kappa_0\rho_0 + 10\kappa_0\rho_2 \\
&+ 40\kappa_0'\rho_0'^* + 40\kappa_0'^*\rho_0' + 4\kappa_2\rho_0 + 2\kappa_2\rho_2 + 8\kappa_2'\rho_0'^* + 8\kappa_2'^*\rho_0' + 12g^4 - 123\alpha g^2,
\end{aligned} \tag{C7}
$$

$$
\begin{aligned}
16\pi^2\beta_{\beta_4} ={}& 16\alpha\beta_4 + 16a_0\beta_4 + 16a_2\beta_4' + 48\beta_4^2 + 80\beta_4\beta_4' + 4\beta_4\lambda_0 - 8\beta_4\lambda_2 + 32\beta_4\lambda_4 + 16\beta_4\lambda_4' \\
&+ 16\beta_4'^2 + 16\beta_4'\lambda_2 + 48\beta_4'\lambda_4 + 640\beta_4'\lambda_4' + 64|\gamma_2|^2 + 24|\zeta|^2 + 96\zeta\varphi^* + 96\zeta^*\varphi + 24|\zeta'|^2 \\
&+ 96\zeta'\varphi'^* + 96\zeta'^*\varphi' + 12g^4 - 123\beta_4 g^2,
\end{aligned} \tag{C8}
$$

$$
\begin{aligned}
16\pi^2\beta_{\beta_4'} ={}& 16\alpha\beta_4' + 16a_0\beta_4' + 2a_2\beta_4 - 4a_2\beta_4' - \beta_4^2 - 28\beta_4\beta_4' + 2\beta_4\lambda_2 + 6\beta_4\lambda_4 + 80\beta_4\lambda_4' \\
&- 124\beta_4'^2 + 4\beta_4'\lambda_0 - 12\beta_4'\lambda_2 + 20\beta_4'\lambda_4 - 144\beta_4'\lambda_4' + 16|\gamma_2|^2 - 48\zeta\varphi^* - 48\zeta^*\varphi \\
&- 48\zeta'\varphi'^* - 48\zeta'^*\varphi' - 3g^4 - 123\beta_4' g^2,
\end{aligned} \tag{C9}
$$

while those for the "old" complex couplings get extended to

$$
\begin{aligned}
16\pi^2\beta_{\gamma_2} ={}& 16\alpha\gamma_2 + 16a_0\gamma_2 + 36a_2\gamma_2 + 28\beta_4\gamma_2 + 56\beta_4'\gamma_2 + 4\gamma_2\lambda_0 + 40\gamma_2\lambda_2 + 180\gamma_2\lambda_4 \\
&+ 160\gamma_2\lambda_4' + 440\gamma_2^*\eta_2 + 12\zeta\zeta' + 2\kappa_2\psi_1 + 4\kappa_2'\psi_0 + 4\kappa_2'^*\psi_2 - 123\gamma_2 g^2,
\end{aligned} \tag{C10}
$$

$$
16\pi^2\beta_{\eta_2} = 16\gamma_2^2 + 24\eta_2\lambda_0 + 160\eta_2\lambda_2 + 600\eta_2\lambda_4 + 640\eta_2\lambda_4' + 4\psi_0\psi_2 + \psi_1^2 - 150\eta_2 g^2. \tag{C11}
$$

For the "new" real couplings of Table II one has

$$
\begin{aligned}
16\pi^2\beta_{h_2} ={}& 56h_2^2 + 16h_2 h_2' + 16h_2'^2 + 72|h_3|^2 + 64|h_4|^2 + 90\kappa_0^2 + 36\kappa_0\kappa_2 + 10\kappa_2^2 + 32|\kappa_2'|^2 \\
&+ 126\rho_0^2 + 126\rho_0\rho_2 + 49\rho_2^2 + 140|\psi_0|^2 + 56|\psi_1|^2 + 140|\psi_2|^2 + \frac{15}{8}g^4 - 54h_2 g^2,
\end{aligned} \tag{C12}
$$

$$
\begin{aligned}
16\pi^2\beta_{h_2'} ={}& 24h_2 h_2' + 40h_2'^2 + 36|h_3|^2 + 224|h_4|^2 + 180|\kappa_0'|^2 + 36\kappa_0'\kappa_2'^* + 36\kappa_0'^*\kappa_2' + 8\kappa_2^2 \\
&+ 4|\kappa_2'|^2 + 252|\rho_0'|^2 - \frac{35}{2}\rho_2^2 - 14|\psi_0|^2 + 70|\psi_1|^2 - 14|\psi_2|^2 + \frac{3}{2}g^4 - 54h_2' g^2,
\end{aligned} \tag{C13}
$$

$$
\begin{aligned}
16\pi^2\beta_{\kappa_0} ={}& 252\alpha\rho_0 + 126\alpha\rho_2 + 376a_0\kappa_0 + 72a_0\kappa_2 + 76a_2\kappa_0 + 8a_2\kappa_2 + 56\beta_4\rho_0 + 28\beta_4\rho_2 \\
&+ 112\beta_4'\rho_0 + 56\beta_4'\rho_2 - 28\gamma_2\psi_1^* - 28\gamma_2^*\psi_1 + 84|\zeta|^2 + 84|\zeta'|^2 + 44h_2\kappa_0 + 8h_2\kappa_2 \\
&+ 8h_2'\kappa_0 + 48h_3\kappa_0'^* + 8h_3\kappa_2'^* + 48h_3^*\kappa_0' + 8h_3^*\kappa_2' + 8\kappa_0^2 + 32|\kappa_0'|^2 + 4\kappa_2^2 + 16|\kappa_2'|^2 + \frac{3}{2}g^4 - 75g^2\kappa_0,
\end{aligned} \tag{C14}
$$

$$
\begin{aligned}
16\pi^2\beta_{\kappa_2} ={}& 16a_0\kappa_2 + 36a_2\kappa_2 + 140\gamma_2\psi_1^* + 140\gamma_2^*\psi_1 - 84|\zeta|^2 - 84|\zeta'|^2 + 4h_2\kappa_2 + 8h_2'\kappa_2 \\
&+ 8h_3\kappa_2'^* + 8h_3^*\kappa_2' + 16\kappa_0\kappa_2 + 32\kappa_0'\kappa_2'^* + 32\kappa_0'^*\kappa_2' + 20\kappa_2^2 + 80|\kappa_2'|^2 + \frac{9}{2}g^4 - 75\kappa_2 g^2,
\end{aligned} \tag{C15}
$$

$$
\begin{aligned}
16\pi^2\beta_{\rho_0} ={}& 180\alpha\kappa_0 + 36\alpha\kappa_2 + 40\beta_4\kappa_0 + 8\beta_4\kappa_2 + 80\beta_4'\kappa_0 + 16\beta_4'\kappa_2 + 24|\zeta|^2 + 44h_2\rho_0 \\
&+ 20h_2\rho_2 + 8h_2'\rho_0 + 8h_2'\rho_2 + 48h_3\rho_0'^* + 48h_3^*\rho_0' + 508\lambda_0\rho_0 + 252\lambda_0\rho_2 + 1220\lambda_2\rho_0 \\
&+ 692\lambda_2\rho_2 + 1340\lambda_4\rho_0 + 788\lambda_4\rho_2 + 2480\lambda_4'\rho_0 + 1232\lambda_4'\rho_2 + 4\rho_0^2 + 16|\rho_0'|^2 + 4\rho_2^2 \\
&+ 24|\psi_1|^2 + 96|\psi_2|^2 + 9984|\varphi|^2 + 1536|\varphi'|^2 + \frac{15}{2}g^4 - 102\rho_0 g^2,
\end{aligned} \tag{C16}
$$

$$
\begin{aligned}
16\pi^2\beta_{\rho_2} ={}& -24|\zeta|^2 + 24|\zeta'|^2 + 4h_2\rho_2 - 8h_2'\rho_2 + 4\lambda_0\rho_2 - 164\lambda_2\rho_2 - 236\lambda_4\rho_2 + 16\lambda_4'\rho_2 \\
&+ 8\rho_0\rho_2 + 4\rho_2^2 + 96|\psi_0|^2 - 96|\psi_2|^2 - 8448|\varphi|^2 + 8448|\varphi'|^2 - 102\rho_2 g^2,
\end{aligned} \tag{C17}
$$

and, similarly, for the "new" complex ones

$$16\pi^2\beta_{h_4} = 24h_2h_4 + 96h'_2h_4 + 18h_3^2 + 90\kappa_0'^2 + 36\kappa_0'\kappa_2' + 18\kappa_2'^2 + 126\rho_0'^2 + 126\psi_0^*\psi_2 - 54h_4g^2, \tag{C18}$$

$$16\pi^2\beta_{h_3} = 72h_2h_3 + 72h'_2h_3 + 144h_3^*h_4 + 180\kappa_0\kappa_0' + 36\kappa_0\kappa_2' + 36\kappa_0'\kappa_2 + 36\kappa_2\kappa_2' + 252\rho_0\rho_0'$$
$$+ 126\rho_0'\rho_2 + 126\psi_0^*\psi_1 + 126\psi_1^*\psi_2 - 54h_3g^2, \tag{C19}$$

$$16\pi^2\beta_{\kappa_0'} = 252\alpha\rho_0' + 376a_0\kappa_0' + 72a_0\kappa_2' + 76a_2\kappa_0' + 8a_2\kappa_2' + 56\beta_4\rho_0' + 112\beta_4'\rho_0' - 28\gamma_2\psi_0^*$$
$$- 28\gamma_2^*\psi_2 + 84\zeta\zeta'^* + 4h_2\kappa_0' + 40h'_2\kappa_0' + 8h'_2\kappa_2' + 24h_3\kappa_0 + 4h_3\kappa_2 + 96h_4\kappa_0'^*$$
$$+ 16h_4\kappa_2'^* + 16\kappa_0\kappa_0' + 8\kappa_2\kappa_2' - 75\kappa_0'g^2, \tag{C20}$$

$$16\pi^2\beta_{\kappa_2'} = 16a_0\kappa_2' + 36a_2\kappa_2' + 140\gamma_2\psi_0^* + 140\gamma_2^*\psi_2 - 84\zeta\zeta'^* + 4h_2\kappa_2' + 4h_3\kappa_2 + 16h_4\kappa_2'^*$$
$$+ 16\kappa_0\kappa_2' + 16\kappa_0'\kappa_2 + 40\kappa_2\kappa_2' - 75\kappa_2'g^2, \tag{C21}$$

$$16\pi^2\beta_{\zeta} = 8\alpha\zeta + 16a_0\zeta - 8a_2\zeta + 64\beta_4\zeta + 160\beta_4\varphi + 48\beta_4'\zeta - 640\beta_4'\varphi + 96\gamma_2\zeta'^* + 8\zeta\kappa_0 - 8\zeta\kappa_2$$
$$+ 2\zeta\rho_0 - 4\zeta\rho_2 + 24\zeta^*\psi_2 + 16\zeta'\kappa_0' - 16\zeta'\kappa_2' + 4\zeta'\rho_0' + 12\zeta'^*\psi_1 - 99\zeta g^2, \tag{C22}$$

$$16\pi^2\beta_{\zeta'} = 8\alpha\zeta' + 16a_0\zeta' - 8a_2\zeta' + 64\beta_4\zeta' + 160\beta_4\varphi' + 48\beta_4'\zeta' - 640\beta_4'\varphi' + 96\gamma_2\zeta^* + 16\zeta\kappa_0'^*$$
$$- 16\zeta\kappa_2'^* + 4\zeta\rho_0'^* + 12\zeta^*\psi_1 + 8\zeta'\kappa_0 - 8\zeta'\kappa_2 + 2\zeta'\rho_0 + 6\zeta'\rho_2 + 24\zeta'^*\psi_0 - 99\zeta'g^2, \tag{C23}$$

$$16\pi^2\beta_{\rho_0'} = 180\alpha\kappa_0' + 36\alpha\kappa_2' + 40\beta_4\kappa_0' + 8\beta_4\kappa_2' + 80\beta_4'\kappa_0' + 16\beta_4'\kappa_2' + 12\zeta\zeta'^* + 4h_2\rho_0' + 40h'_2\rho_0'$$
$$+ 24h_3\rho_0 + 12h_3\rho_2 + 96h_4\rho_0'^* + 508\lambda_0\rho_0' + 1220\lambda_2\rho_0' + 1340\lambda_4\rho_0' + 2480\lambda_4'\rho_0'$$
$$+ 8\rho_0\rho_0' + 4\rho_0'\rho_2 + 24\psi_0^*\psi_1 + 24\psi_1^*\psi_2 + 5760\varphi\varphi'^* - 102\rho_0'g^2, \tag{C24}$$

$$16\pi^2\beta_{\psi_2} = 32\gamma_2\kappa_2' + 12\zeta^2 + 440\eta_2\psi_0^* + 4h_2\psi_2 + 4h_3\psi_1 + 16h_4\psi_0 + 4\lambda_0\psi_2 + 40\lambda_2\psi_2 + 180\lambda_4\psi_2$$
$$+ 160\lambda_4'\psi_2 + 8\rho_0\psi_2 + 8\rho_0'\psi_1 - 16\rho_2\psi_2 + 3840\varphi^2 - 102\psi_2g^2, \tag{C25}$$

$$16\pi^2\beta_{\psi_1} = 32\gamma_2\kappa_2 + 24\zeta\zeta' + 440\eta_2\psi_1^* + 4h_2\psi_1 + 8h'_2\psi_1 + 8h_3\psi_0 + 8h_3^*\psi_2 + 4\lambda_0\psi_1 + 40\lambda_2\psi_1$$
$$+ 180\lambda_4\psi_1 + 160\lambda_4'\psi_1 + 8\rho_0\psi_1 + 16\rho_0'\psi_0 + 16\rho_0'^*\psi_2 + 4\rho_2\psi_1 + 7680\varphi\varphi' - 102\psi_1g^2, \tag{C26}$$

$$16\pi^2\beta_{\psi_0} = 32\gamma_2\kappa_2'^* + 12\zeta'^2 + 440\eta_2\psi_2^* + 4h_2\psi_0 + 4h_3^*\psi_1 + 16h_4^*\psi_2 + 4\lambda_0\psi_0 + 40\lambda_2\psi_0 + 180\lambda_4\psi_0$$
$$+ 160\lambda_4'\psi_0 + 8\rho_0\psi_0 + 8\rho_0'^*\psi_1 + 24\rho_2\psi_0 + 3840\varphi'^2 - 102\psi_0g^2, \tag{C27}$$

$$16\pi^2\beta_{\varphi} = \beta_4\zeta - 4\beta_4'\zeta + 12\lambda_0\varphi - 8\lambda_2\varphi + 40\lambda_4\varphi - 656\lambda_4'\varphi + 6\rho_0\varphi + 12\rho_0'\varphi' - 8\rho_2\varphi + 48\psi_2\varphi^*$$
$$+ 24\psi_1\varphi'^* - 126\varphi g^2, \tag{C28}$$

$$16\pi^2\beta_{\varphi'} = \beta_4\zeta' - 4\beta_4'\zeta' + 12\lambda_0\varphi' - 8\lambda_2\varphi' + 40\lambda_4\varphi' - 656\lambda_4'\varphi' + 6\rho_0\varphi' + 12\rho_0'^*\varphi + 14\rho_2\varphi'$$
$$+ 24\psi_1\varphi^* + 48\psi_0\varphi'^* - 126\varphi'g^2. \tag{C29}$$

Several remarks may again be worth making here:

(1) In the full $\mathbf{45} \oplus \mathbf{126} \oplus \mathbf{10}_{\mathbb{C}}$ scenario the β functions of the "old" couplings relevant for the $\mathbf{45} \oplus \mathbf{126}$ Higgs model of Ref. [13] receive contributions from the "new" couplings as well. Note that some minor errors present in the expressions for β_{λ_2}, β_{λ_4}, β_{γ_2}, and β_{η_2} in [13] have been corrected. It has also been verified that the corresponding changes have only very minor quantitative effects and the results of [13] remain unchanged.

(2) The beta functions of all real scalar couplings are manifestly real, as they should be.

(3) The beta functions of complex couplings (associated to the presence of two complex scalar representations Σ and H) exhibit the standard patterns associated to phase redefinitions of complex representations, which greatly restricts the form the individual terms within might take. To illustrate this, one can consider, e.g., the phase redefinition of $\Sigma \to e^{i\epsilon}\Sigma$; absorbing the phases that appear in the scalar potential into the

TABLE VIII. Nontrivial charge assignments of the dimensionless scalar couplings under $U(1)_\Sigma \times U(1)_H$.

	γ_2	η_2	h_4	h_3	κ'_0	κ'_2	ζ
$U(1)_\Sigma$	-2	-4	$+0$	$+0$	$+0$	$+0$	-1
$U(1)_H$	$+0$	$+0$	-4	-2	-2	-2	-1

	ζ'	ρ'_0	ψ_2	ψ_1	ψ_0	φ	φ'
$U(1)_\Sigma$	-1	$+0$	-2	-2	-2	-1	-1
$U(1)_H$	$+1$	-2	-2	$+0$	$+2$	-1	$+1$

(complex) couplings, one can verify readily that the system of the RGEs above will change consistently with this (unphysical) transformation. A systematic way to track this is to define a $U(1)_\Sigma$ transformation, under which the charge of Σ is defined to be $+1$, with all other scalar representations remaining neutral and the charges of all couplings (playing the role of spurions) set so that the scalar potential of Eqs. (2)–(7) is $U(1)_\Sigma$ invariant. Analogously, one can define another phase transformation $U(1)_H$ acting solely on H (with the associated charge $+1$) and set the $U(1)_H$ charges of all couplings so that the scalar potential is again $U(1)_H$ invariant. The corresponding $U(1)_\Sigma \times U(1)_H$ charges of all dimensionless scalar couplings are shown in Table VIII. Since each beta function β_λ in the list above should have the same $U(1)_\Sigma \times U(1)_H$ charge as the corresponding coupling λ, all terms in β_λ must have that same charge; for instance, all terms of β_{γ_2} must have the $U(1)_\Sigma \times U(1)_H$ charge $(-2, 0)$, as they do. One can indeed confirm that all structures in Eqs. (C2)–(C29) do adhere to this rule. This pattern leads to a number of interesting consequences:

(a) Given the information in Table VIII, the scalar potential (with couplings promoted to fields) is invariant under $U(1)_\Sigma \times U(1)_H$, and hence also under any linear combination of the two $U(1)$

factors. In particular, we can define the PQ charge of a field/coupling x as

$$[x]_{PQ} := 2[x]_\Sigma - 2[x]_H, \qquad (C30)$$

which is indeed consistent with Eq. (35). This also implies that the β-functions above must preserve the PQ charge thus defined.

(b) Coming back to the plain scalar potential with couplings interpreted as mere parameters rather than spurions, only those with a zero PQ charge are allowed if $U(1)_{PQ}$ is supposed to be a good symmetry of the model. In such a case, besides the real couplings, the only allowed complex ones are ζ, ψ_2, and φ; at the same time, the system of RGEs consistently reduces to a subsystem for these PQ-allowed couplings only, while the beta functions of all the remaining (PQ-charged) couplings vanish identically. Analogous considerations apply for an alternative PQ-like charge $[x]_{PQ'} := 2[x]_\Sigma + 2[x]_H$, or more generally for any linear combination of the primary charges $U(1)_\Sigma$ and $U(1)_H$.

(c) A coupling has a nontrivial $U(1)_\Sigma \times U(1)_H$ charge if and only if it is complex. Since the gauge coupling g is real, it must have charge $(0,0)$, and thus the g^4 contributions must vanish in the β functions of all complex couplings, as confirmed by the results above. Interestingly, the g^4 term also vanishes in the β function of the real parameter ρ_2 with no specific insight from this type of arguments.

(d) Charge conservation provides nontrivial constraints in all beta functions, including those for real couplings. If a coupling is real, then its beta function must be both real and $U(1)_\Sigma \times U(1)_H$ neutral, e.g., a contribution like $\kappa'_0 \kappa'^*_2 +$ c.c. is allowed but $\kappa'_0 \kappa'_2 +$ c.c. is not.

[1] S. Bertolini, L. Di Luzio, and M. Malinsky, Phys. Rev. D **81**, 035015 (2010).

[2] S. Bertolini, L. Di Luzio, and M. Malinsky, Phys. Rev. D **85**, 095014 (2012).

[3] S. Bertolini, L. Di Luzio, and M. Malinsky, Phys. Rev. D **87**, 085020 (2013).

[4] H. Kolešová and M. Malinský, Phys. Rev. D **90**, 115001 (2014).

[5] T. D. Brennan, Phys. Rev. D **95**, 065008 (2017).

[6] K. S. Babu, B. Bajc, and S. Saad, J. High Energy Phys. 02 (2017) 136.

[7] K. S. Babu, B. Bajc, and S. Saad, Phys. Rev. D **94**, 015030 (2016).

[8] L. Gráf, M. Malinský, T. Mede, and V. Susič, Phys. Rev. D **95**, 075007 (2017).

[9] J. Schwichtenberg, Eur. Phys. J. C **79**, 351 (2019).

[10] L. Di Luzio, J. High Energy Phys. 11 (2020) 074.
[11] T. Ohlsson, M. Pernow, and E. Sönnerlind, Eur. Phys. J. C **80,** 1089 (2020).
[12] S. F. King, S. Pascoli, J. Turner, and Y.-L. Zhou, J. High Energy Phys. 10 (2021) 225.
[13] K. Jarkovská, M. Malinský, T. Mede, and V. Susič, Phys. Rev. D **105,** 095003 (2022).
[14] K. Abe et al., arXiv:1109.3262.
[15] K. Abe et al. (Hyper-Kamiokande Collaboration), arXiv:1805.04163.
[16] R. Acciarri et al. (DUNE Collaboration), arXiv:1512.06148.
[17] R. Acciarri et al. (DUNE Collaboration), arXiv:1601.05471.
[18] Y. Aoki, T. Izubuchi, E. Shintani, and A. Soni, Phys. Rev. D **96,** 014506 (2017).
[19] H. Kolešová and M. Malinský, Phys. Rev. D **99,** 035005 (2019).
[20] C. T. Hill, Phys. Lett. **135B,** 47 (1984).
[21] Q. Shafi and C. Wetterich, Phys. Rev. Lett. **52,** 875 (1984).
[22] X. Calmet, S. D. H. Hsu, and D. Reeb, Phys. Rev. Lett. **101,** 171802 (2008).
[23] F. Buccella, H. Ruegg, and C. A. Savoy, Phys. Lett. **94B,** 491 (1980).
[24] M. Yasue, Phys. Rev. D **24,** 1005 (1981).
[25] G. Anastaze, J. P. Derendinger, and F. Buccella, Z. Phys. C **20,** 269 (1983).
[26] K. S. Babu and E. Ma, Phys. Rev. D **31,** 2316 (1985).
[27] F. del Aguila and L. E. Ibanez, Nucl. Phys. **B177,** 60 (1981).
[28] R. N. Mohapatra and G. Senjanovic, Phys. Rev. D **27,** 1601 (1983).
[29] S. Bertolini, L. Di Luzio, and M. Malinsky, Phys. Rev. D **80,** 015013 (2009).
[30] J. M. Gipson and R. E. Marshak, Phys. Rev. D **31,** 1705 (1985).
[31] N. G. Deshpande, E. Keith, and P. B. Pal, Phys. Rev. D **47,** 2892 (1993).
[32] S. Dimopoulos and H. M. Georgi, Phys. Lett. **140B,** 67 (1984).
[33] P. Langacker, Phys. Rep. **72,** 185 (1981).
[34] S. Antusch, C. Hohl, and V. Susič, J. High Energy Phys. 02 (2020) 086.
[35] L. Lehman and A. Martin, Phys. Rev. D **91,** 105014 (2015).
[36] B. Henning, X. Lu, T. Melia, and H. Murayama, J. High Energy Phys. 10 (2017) 199.
[37] R. Feger and T. W. Kephart, Comput. Phys. Commun. **192,** 166 (2015).
[38] R. Feger, T. W. Kephart, and R. J. Saskowski, Comput. Phys. Commun. **257,** 107490 (2020).
[39] B. Bajc, A. Melfo, G. Senjanovic, and F. Vissani, Phys. Rev. D **73,** 055001 (2006).
[40] K. S. Babu and R. N. Mohapatra, Phys. Rev. Lett. **70,** 2845 (1993).
[41] A. S. Joshipura and K. M. Patel, Phys. Rev. D **83,** 095002 (2011).
[42] G. Altarelli and D. Meloni, J. High Energy Phys. 08 (2013) 021.
[43] A. Dueck and W. Rodejohann, J. High Energy Phys. 09 (2013) 024.
[44] K. S. Babu and S. Khan, Phys. Rev. D **92,** 075018 (2015).
[45] S. M. Boucenna, T. Ohlsson, and M. Pernow, Phys. Lett. B **792,** 251 (2019); **797,** 134902(E) (2019).
[46] T. Ohlsson and M. Pernow, J. High Energy Phys. 06 (2019) 085.
[47] V. S. Mummidi and K. M. Patel, J. High Energy Phys. 12 (2021) 042.
[48] D. Meloni, T. Ohlsson, and S. Riad, J. High Energy Phys. 12 (2014) 052.
[49] D. Meloni, T. Ohlsson, and S. Riad, J. High Energy Phys. 03 (2017) 045.
[50] T. Ohlsson and M. Pernow, J. High Energy Phys. 11 (2018) 028.
[51] T. Fukuyama, N. Okada, and H. M. Tran, Nucl. Phys. **B954,** 114992 (2020).
[52] R. Slansky, Phys. Rep. **79,** 1 (1981).
[53] S. Bertolini, T. Schwetz, and M. Malinsky, Phys. Rev. D **73,** 115012 (2006).
[54] T. Deppisch, S. Schacht, and M. Spinrath, J. High Energy Phys. 01 (2019) 005.
[55] M. Georgioudakis and V. Plevris, Front. Built Environ. **6,** 102 (2020).
[56] S. A. R. Ellis and J. D. Wells, Phys. Rev. D **91,** 075016 (2015).
[57] S. Weinberg, Phys. Lett. **91B,** 51 (1980).
[58] L. J. Hall, Nucl. Phys. **B178,** 75 (1981).
[59] M. Tanabashi et al. (Particle Data Group), Phys. Rev. D **98,** 030001 (2018).
[60] W. J. Marciano, Annu. Rev. Nucl. Part. Sci. **41,** 469 (1991).
[61] J. H. Kuhn and M. Steinhauser, Phys. Lett. B **437,** 425 (1998).
[62] W. Martens, L. Mihaila, J. Salomon, and M. Steinhauser, Phys. Rev. D **82,** 095013 (2010).
[63] C. Sturm, Nucl. Phys. **B874,** 698 (2013).
[64] P. A. Zyla et al. (Particle Data Group), Prog. Theor. Exp. Phys. **2020,** 083C01 (2020).